

Development of a Soft Robotic Exosuit for Knee Flexion Assistance

by

Ibrahim Mohammed Ibrahim Hasan

A Thesis Presented in Partial Fulfillment
of the Requirements for the Degree
Master of Science

Approved May 2021 by the
Graduate Supervisory Committee:

Wenlong Zhang, Chair
Daniel Aukes
Troy McDaniel

ARIZONA STATE UNIVERSITY

August 2021

ABSTRACT

The knee joint has essential functions to support the body weight and maintain normal walking. Neurological diseases like stroke and musculoskeletal disorders like osteoarthritis can affect the function of the knee. Besides physical therapy, robot-assisted therapy using wearable exoskeletons and exosuits has shown the potential as an efficient therapy that helps patients restore their limbs' functions. Exoskeletons and exosuits are being developed for either human performance augmentation or medical purposes like rehabilitation. Although, the research on exoskeletons started early before exosuits, the research and development on exosuits have recently grown rapidly as exosuits have advantages that exoskeletons lack. The objective of this research is to develop a soft exosuit for knee flexion assistance and validate its ability to reduce the EMG activity of the knee flexor muscles. The exosuit has been developed with a novel soft fabric actuator and novel 3D printed adjustable braces to attach the actuator aligned with the knee. A torque analytical model has been derived and validated experimentally to characterize and predict the torque output of the actuator. In addition to that, the actuator's deflation and inflation time has been experimentally characterized and a controller has been implemented and the exosuit has been tested on a healthy human subject.

It is found that the analytical torque model succeeded to predict the torque output in flexion angle range from 0° to 60° more precisely than analytical models in the literature. Deviations existed beyond 60° might have happened because some factors like fabric extensibility and actuator's bending behavior. After human testing, results showed that, for the human subject tested, the exosuit gave the best performance when the controller was

tuned to inflate at 31.9 % of the gait cycle. At this inflation timing, the biceps femoris, the semitendinosus and the vastus lateralis muscles showed average electromyography (EMG) reduction of - 32.02 %, - 23.05 % and - 2.85 % respectively. Finally, it is concluded that the developed exosuit may assist the knee flexion of more diverse healthy human subjects and it may potentially be used in the future in human performance augmentation and rehabilitation of people with disabilities.

DEDICATION

To my Dad, and stroke fighters who suffer a lot...

To my mom, the real hero behind the scenes...

I love you both...

ACKNOWLEDGMENTS

First, I would like to thank God for guiding and surrounding me during this journey. This work would not have come true without his guidance and mercy. May Allah bless me to be thankful to his limitless blessings.

I would like to thank my advisor, Professor Wenlong Zhang, for being helpful, supportive, and insightful to guide the research towards novel contributions in the field. Many thanks to my committee members, Professor Daniel Aukes and Professor Troy McDaniel, for being understanding and helpful since day one. I would like also to thank my colleague Emiliano Quinones for lending his helping hand whenever I needed. Also, many thanks to my colleagues Pham Huy Nguyen and Zhi Qiao for their advice, that helped me a lot. Also, many thanks for Deepit Arora, Karishma Patnaik and Mostafa Rezayat for helping me during the experiments and motion capture.

Special thanks to my family. My father and my mother who are the reason I am, and who never stopped to show me love and faith. My brother Ahmed who is always there holding my back and taking the responsibility whenever it is. My sisters Amira and Amany and their kids, Menna, Raghad, Mahmoud, Adam and Aser. Thanks for being there all over the journey making me smile when it was hard. I love you all. Finally, to my sweetheart and my fiancée Israa, thanks for being always loving, trustful and honest. Thanks for being home. Thanks that you always believe in me. Things are easier because you are always here. I love you.

Ibrahim Hasan

May 14, 2021

TABLE OF CONTENTS

	Page
LIST OF TABLES.....	vii
LIST OF FIGURES.....	viii
CHAPTER	
1 INTRODUCTION.....	1
1.1. Motivation.....	1
1.2. Wearable Robotic Devices.....	2
1.3. Knee Exosuits.....	4
1.4. Research Gaps and Thesis Objective.....	7
2 EXOSUIT DESIGN.....	9
2.1. Actuator Concept Development.....	9
2.2. CPIA Description and Principle of Operation.....	14
2.3. Braces Design.....	17
2.3.1. Fabric Brace.....	17
2.3.2. 3D Printed Brace.....	19
2.4. Final Exosuit.....	21
3 CHARACTERIZATION.....	25
3.1. Knee Joint Biomechanical Requirements.....	25
3.2. Torque Characterization.....	27
3.2.1. Analytical Model.....	28
3.2.2. Experimental Model.....	32

CHAPTER	Page
3.2.3. Torque-Pressure Results and Discussion	34
3.2.4. Torque-Angle Results and Discussion.....	43
3.2.5. Analytical Model Limitations	45
3.3. Inflation and Deflation Characterization	51
4 CONTROL AND HUMAN TESTING	55
4.1. Control Strategy	55
4.2. Hardware Setup and Components	57
4.3. Human Testing.....	58
4.3.1. Testing Protocol	58
4.3.2. Human Testing Setup.....	60
4.3.3. Data Processing.....	60
4.3.4. Results.....	62
4.3.5. Results Discussion	69
5 CONCLUSIONS	74
6 FUTURE WORK	77
REFERENCES	79
APPENDIX	
A DECISION MATRICES	82

LIST OF TABLES

Table	Page
2.1 Decision Matrix to Evaluate the Concepts.....	13
3.1 Summary of Biomechanical Knee Flexion Torque Requirements.	25
3.2. Inflation and Deflation Durations of The CPIA.	54
4.1. Information of The Human Subject.....	62

LIST OF FIGURES

Figure	Page
2.1. Demonstration of the PAM Concept on the Knee Joint.	10
2.2. Demonstration of the Accordion-Inspired Actuator on the Knee.....	10
2.3. Demonstration of the CPIA on the Knee.....	11
2.4. CPIA Actuator's Structure.....	15
2.5. CPIA in Inflated Folded State.....	16
2.6. Exosuit with Soft Fabric Braces.	18
2.7. Top View of Tissue Stress due to Actuator Inflation with Fabric Braces.	19
2.8. Thigh's 3D Printed Modular Brace Drawings.....	20
2.9. Shank's 3D Printed Modular Brace Drawings.	21
2.10. Exosuit Demonstration with 3D Printed Braces.	22
2.11. Front View of Real Integration of the Exosuit In Deflated State.	23
2.12. Front View of the Real Integration of the Exosuit in Inflated State.	24
3.1 Experimental Torque Values of the Candidate CPIA at 20 psi.	27
3.2. PIA in Folded State.....	29
3.3. (a) (Nesler et al., 2018), (b) Experimental Observation.....	30
3.4. Free Body Diagram of the PIA in Folded State.....	30
3.5. Actuator's Trigonometry and Kinematics.....	32
3.6. Experimental Test Rig.	33
3.7. Torque Characterization at 0° Flexion Angle.....	35
3.8. Torque Characterization at 10° Flexion Angle.....	35

Figure	Page
3.9. Torque Characterization at 20° Flexion Angle.....	36
3.10. Torque Characterization at 30° Flexion Angle.....	36
3.11. Torque Characterization at 40° Flexion Angle.....	37
3.12. Torque Characterization at 50° Flexion Angle.....	37
3.13. Torque Characterization at 60° Flexion Angle.....	38
3.14. Torque Characterization at 70° Flexion Angle.....	38
3.15. Torque Characterization at 80° Flexion Angle.....	39
3.16. Torque Characterization at 90° Flexion Angle.....	39
3.17. Change in folded volume with buckling angle.....	44
3.18. Torque-Angle Results at 5 psi.....	46
3.19. Torque-Angle Results at 10 psi.....	46
3.20. Torque-Angle Results at 15 psi.....	47
3.21. Torque-Angle Results at 20 psi.....	47
3.22. Torque-Angle Results at 25 psi.....	48
3.23. Torque-Angle Results at 30 psi.....	48
3.24. Torque-Angle Results at 35 psi.....	49
3.25. Folded CPIA at 0° Flexion Angle.....	49
3.26. Folded CPIA at 30° Flexion Angle.....	50
3.27. Folded CPIA at 60° Flexion Angle.....	50
3.28. Folded CPIA at 90° Flexion Angle.....	51
3.29. Pressure Response of the CPIA.....	53

Figure	Page
4.1. Control Strategy.....	55
4.2. Hardware Setup and Components.....	58
4.3. Human Testing Setup.....	61
4.4. EMG of Biceps Femoris vs Actuator’s Pressure at 35.6 % GC Delay.....	63
4.5. EMG of Semitendinosus Vs Actuator’s Pressure at 35.6 % GC Delay.....	63
4.6. EMG of Vastus Lateralis Vs Actuator’s Pressure at 35.6 % GC Delay.	64
4.7. EMG of Biceps Femoris Vs Actuator’s Pressure at 31.9 % GC Delay.	64
4.8. EMG of Semitendinosus Vs Actuator’s Pressure at 31.9 % GC Delay.....	65
4.9. EMG of Vastus Lateralis Vs Actuators Pressure at 31.9 % GC Delay.....	65
4.10. EMG of Biceps Femoris Vs Actuator’s Pressure at 28.1 % GC Delay.	66
4.11. EMG of Semitendinosus Vs Actuator’s Pressure at 28.1 % GC Delay.....	66
4.12. EMG of Vastus Lateralis Vs Actuator’s Pressure at 28.1 % GC Delay.	67
4.13. EMG of Biceps Femoris Vs Actuator’s Pressure at 24.78 % GC Delay.	67
4.14. EMG of Semitendinosus Vs Actuator’s Pressure at 24.78 % GC Delay.....	68
4.15. EMG of Vastus Lateralis Vs Actuator’s Pressure at 24.78 % GC Delay.	68
4.16. EMG Percentage Change of the Inactive Trial Compared to the Baseline.....	69
4.17. EMG Percent Change of the Active Trial Compared to the Baseline.	70
4.18. EMG Percent Change Compared of the Active Trial to the Inactive.	72

CHAPTER 1

INTRODUCTION

1.1. Motivation

The knee joint has functions that are essential to perform different activities like walking, running, sitting, and standing. It has flexion and extension motion in the sagittal plane that are mostly used in activities like normal walking and standing up. It also has rotation internally and externally in the horizontal plane that is important in activities like running and changing direction. In normal walking, the knee either supports the body weight or absorbs the heel strike shock or assists the lower limb to swing and keep the forward progression of the legs natural (Mansfield & Neumann, 2019; Shamaei et al., 2014). In other words, the knee flexes momentarily in the early stance phase to absorb the heel strike shock while in the swing phase it exhibits large flexion to make to clearance for leg swing (Zoss et al., 2006).

The loss of the knee functions is caused by either neurological or musculoskeletal causes. The neurological disorders cause disabilities such that the nervous system which is responsible for coordinating the joint's function is affected. Stroke, spinal cord injury (SCI) and cerebral palsy (CP) are the most common neurological disorders that lead to motor disabilities. According to (Armour et al., 2016), stroke is the first leading cause of disabilities in the United States such that it affects 33.7 % of people with paralysis while SCI and CP come after such that they affect 27.3 % and 8.3 % of the paralyzed population consequently.

On the other hand, the musculoskeletal disorders lead to losing the knee function because of diseases or injuries that happen to the knee biomechanical structure. Knee osteoarthritis, anterior cruciate ligament (ACL) injury, and meniscus injury are all classified as musculoskeletal disorders. According to Centers for Disease Control and Prevention (CDC) there are over 32.5 million affected by osteoarthritis. Also in study (Mall et al., 2014), it has been shown that the incidence of ACL has been increased from 86,687 in 1994 to 129,836 in 2006 in the United States.

In addition to medical treatment, physical therapy programs and rehabilitation training are followed to restore the joints' functions and the motor ability. Rehabilitation is expected to restore the range of motion of the joint, strengthen the muscles and reduce the pain and swelling if exist. There are two types of rehabilitative exercises. The first kind is the clinical supervised rehabilitation that is performed by physical therapists in clinics. The second type is the exercises that are done at home. To have an effective physical therapy, the rehabilitation exercises should be designed to be task-oriented, repetitive, and encouraging to the patients to exhibit active participation. In addition to that, achieving home rehabilitation that can replicate the clinical rehabilitation is another factor that leads to more efficient therapy. Therefore, the attention has been paid for years to develop robotic devices that can provide efficient rehabilitation both in clinic and at home.

1.2. Wearable Robotic Devices

Robot-assisted therapies have shown a great potential for more effective and efficient therapy than the conventional physical therapies. Study (Fasoli et al., 2012) concluded that, robot-assisted therapy is a promising technique that has significant

improvements on the functions of both upper limb and lower limb for the neurologically impaired due to stroke or CP. Moreover, wearable robotic devices have attracted the attention of researchers as potential efficient assistive and rehabilitative devices.

Wearable robotic devices can be classified as exoskeletons and exosuits. Exoskeletons consist of series of rigid elements that are connected by mechanical joints like revolute, prismatic or ball and socket. This mechanical structure forms an external skeletal system works in parallel with the human body's skeletal system. Exoskeletons deliver motion to the human's joints by using electric motors, hydraulic, or pneumatic actuators. These different actuators play the role of the muscles of the human body. During the past few decades, there were large number of studies that have been performed to design compact and efficient exoskeletons for human use. Nevertheless, designing an anthropomorphic, light in weight and easy-to-wear exoskeletons is still an ongoing challenge that faces scientific community.

On the other hand, exosuits are conceptually developed to rely on the human skeleton to transfer motion to the joints. This is achieved by attaching external cable-driven or textile soft actuators that act as an external muscular system that powers the joints simultaneously with the human muscular system. Soft exosuits are mainly developed to actuate in parallel with the human muscles' not to provide full forces required to human walking. Textile exosuits have many advantages like wearer comfort, adjustability to fit many users, low profiles and mass reduction around distal components which increases the efficiency. Studies in the literature have demonstrated that assistive forces that are relatively low can significantly reduce the metabolic cost, and the metabolic cost reduction

is proportional to the level of assistance (Sanchez et al., 2020). Therefore, for these advantages, exosuits have attracted the attention of researchers as potential effective rehabilitative and assistive wearable devices.

1.3. Knee Exosuits

In the literature, there are several cable-driven and pneumatic exosuits developed for knee rehabilitation and assistance. Many cable-driven exosuits showed the potential to reduce the knee power and the EMG activity of the knee muscles. In study (Huang et al., 2020), the authors developed a biologically-inspired cable driven exosuit for knee extension assistance during stair ascent. A Bowden cable is placed in front of the knee to mimic the function of the quadriceps. The exosuit has been tested on human subjects and showed 10.92% reduction in the knee moment and 30% reduction in the knee power. In (Park et al., 2020), a cable driven hinge-free exosuit has been developed to assist knee extension as well. The exosuit has been tested on 6 healthy human subjects walking uphill and downhill on a 10° tilted treadmill. The results showed that the exosuit reduced the biological power of the knee joint which shows its potential as an assistive and rehabilitation device. Study (Lee et al., 2020) proposed a wire-driven exosuit to support the knee joint during stair ascent and descent. The authors have implemented an admittance control strategy based on gait analysis and force control to aid the wearer. The muscle activity has been measured and analyzed for different subjects with and without the exosuit. Out of this study, it was concluded that the exosuit has led to a reduction in the overall muscle activity up to 47 % for the rectus femoris muscle during ascent and 31 % during

descent. The muscle activity of the gastrocnemius and biceps femoris did not show any noticeable change.

Pneumatic exosuits have also shown the potential to assist the knee and reduce muscles activity during activities like normal walking, sitting, and standing. Study (Veale et al., 2020) introduced a soft exosuit for knee extension during sit-to-stand. The exosuit employs a pleated pneumatic interference actuator (PPIA) that is compliant, lightweight and integrable to clothing. The actuator consists of a fabric reinforced rubber tube that generates torque when buckles. To achieve the torque requirement for knee extension during sit-to-stand, multiple PPIA actuators have been integrated together. Results showed that, the configuration was able to generate a torque of 324 Nm at 320 KPa and flexion angle of 82 degrees. This torque has exceeded the torque required during sit-to-stand which is 180 Nm. The authors intend to test the exosuit on humans in the future. The study concluded that, more development is needed to make the PPIA less bulky and increase the accuracy of the analytical model. In addition to that, future work should address maximizing the speed, power and flexibility and minimizing bulk. (Fang et al., 2018, 2020) introduced a novel accordion-inspired actuator for knee extension assistance. The exosuit is inspired by the Chinese folding fans and is made of thermoplastic polyurethane (TPU) fabric materials. The actuator has been modeled analytically and validated experimentally. It has also been tested on 5 human subjects. The electromyography (EMG) results showed ability of the exosuit to assist extension of the knee. Furthermore, the authors concluded that, the biomechanical energy of the knee joint can be harvested and used in assisting the knee joint by adjusting the inner pressure of the exosuit.

The Robotics and Intelligent Systems Laboratory at Arizona State University has also introduced a novel soft inflatable knee extension exosuit (Sridar et al., 2017, 2020). The exosuit incorporated inflatable pneumatic actuators made of heat sealable TPU with I and O cross-sections. The authors introduced theoretical analysis based on Euler-Bernulli beam theory to validate the hypothesis that actuators with I cross sections can withstand higher forces than actuators with O cross section. They also performed experimental testing by measuring the force output of the knee exosuit using the two different actuators on a universal testing Instron machine. In the experimental testing, the exosuit was mounted on a biologically inspired knee joint to mimic the human joint. As hypothesized, the actuators with I cross-section have produced higher force output than the actuators with O cross-section. Then, the exosuit has been tested on healthy human subjects to test its ability to reduce the muscles' activity during the swing phase of walking. The exosuit is activated during the swing phase by using a smart shoe that employs soft-silicone insole with embedded force resistive resistors. The muscle activity was measured by using sEMG sensors placed on the rectus femoris muscle group. The results showed that, there is 7% reduction in the muscle activity which shows the potential of the proposed exosuit as a rehabilitation device. In future work, the authors intend to address testing the exosuit on humans on both active and inactive conditions to have more comprehensive evaluation. Also, developing computational models to such actuators to test variations like different materials and cross-section is yet to be developed. Another challenge is increasing the inflation and the deflation rate of the actuator to have better timing for assistance.

1.4. Research Gaps and Thesis Objective

Cable-driven exosuits have shown the potential to both assist knee flexion and extension motion. On the other hand, cable-driven mechanisms represent a challenge to such exosuits because transmissions mechanisms are required which makes the exosuit bulky and not anthropomorphic. In addition to that, cable-driven mechanisms require specific casings to maintain safe interaction with the human. Finally, cable-driven exosuits require auxiliary equipment like electrical motors and batteries which makes it challenging to be wearable.

Although pneumatic exosuits have the same disadvantage of requiring bulky auxiliary equipment like compressors and valves, they show interesting advantages that cable-driven exosuit lack. Soft pneumatic exosuit rely on soft actuator to generate the motion requirements. This gives the advantage of having low profile, being light in weight, compliant and more transparent to the human body. In addition to that, pneumatic actuators have shown the potential as powerful actuators with high power to weight ratio (Li et al., 2017; Nesler et al., 2018; Sridar et al., 2017). Moreover, pneumatic actuators are safer to interact with the human than cable-driven mechanisms that have relative frictional motion that may cause discomfort to the wearer.

As pneumatic soft textile exosuits have such advantages that make them promising wearable assistive and rehabilitative devices, the attention in this research has been narrowed down to address a research gap add a novel contribution in that scope. According to our knowledge, all the soft exosuit developed for the knee joints are dedicated to assisting only the extension motion of the knee joint. This obviously represents a research

gap as the knee flexion has crucial physiological and biomechanical functions as discussed in section 1.1. Hence, the objective of this research is focused on developing a soft pneumatic exosuit for knee flexion assistance.

CHAPTER 2

EXOSUIT DESIGN

2.1. Actuator Concept Development

The flexion motion of the knee joint is curvilinear, therefore the exosuit should provide actuation that is analogous to that produced by the knee flexors, the hamstrings muscles. Pneumatic actuators have the advantages of being light in weight, powerful and compliant in deflated state. Therefore, the focus is paid to developing a pneumatic actuator that can achieve the kinematic and kinetic knee flexion requirements. By looking at the literature, we have been inspired by some ideas for pneumatic actuator as potential knee flexion actuators. These ideas are all pneumatic, however they differ in principle of operation.

The first concept is based on developing a contractile pneumatic artificial muscle (PAM) that either works on positive pressures like pleated artificial muscles or negative pressure like fluid-driven origami-inspired artificial muscles (FOAMs). The flexion motion is to be generated by mounting the actuator on the back of the leg and anchoring its ends to the thigh and shank so that when it contracts it flexes the knee as indicated in Figure 2.1. The second concept generates the knee flexion by placing actuators such as the accordion actuator inspired by Chinese fans (Fang et al., 2020) or the multi-chamber actuator developed for elbow lifting assistance (Thalman et al., 2018) to be placed in front of the knee joint such that it flexes the joint when it is inflated. Figure 2.2 is an illustration of the concept. This kind of actuator consists of a group of fabric heat-sealed air cavities that are stitched along curved paths such that when the cavities are filled with air, they push against

each other to form a curved stiff actuator that braces the knee in the flexed position as demonstrated in Figure 2.2.

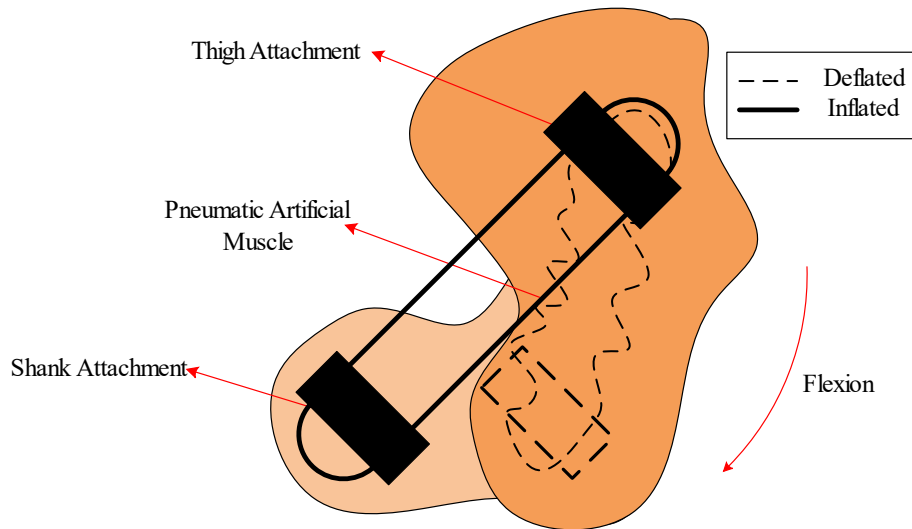


Figure 2.1. Demonstration of the PAM Concept on the Knee Joint.

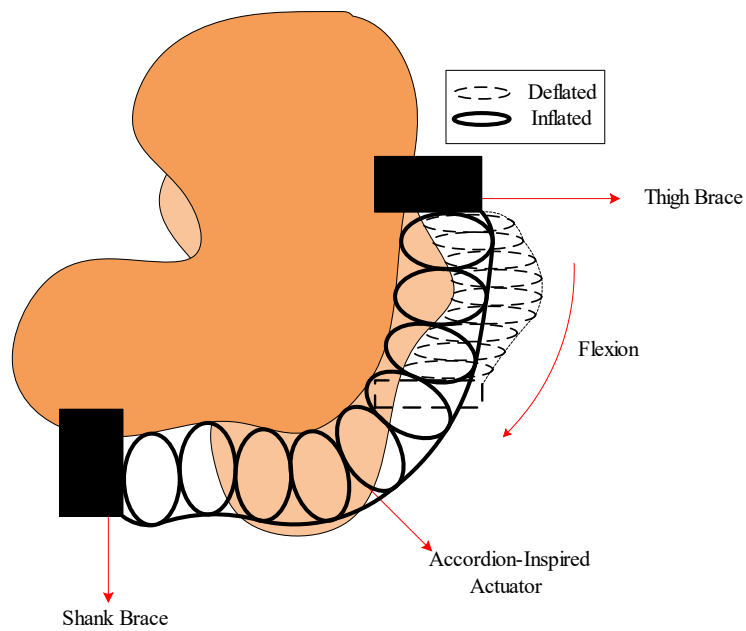


Figure 2.2. Demonstration of the Accordion-Inspired Actuator on the Knee.

The third concept is to develop a curved pneumatic interference actuator (CPIA) that has a curvature matched with the knee's flexed position. If the actuator is inflated, the actuator is stiff. If it is aligned with the thigh and shank, the actuator's stiffness will keep the knee flexed if it is inflated. This behavior is like placing a torsional spring at the knee joint such that its initial uncompressed state is adjusted when the knee is flexed. Any force happens to extend the knee, the torsional spring will act by a torque in the opposite direction to restore the knee back to the flexed initial position. Figure 2.3 shows a demonstration of the concept.

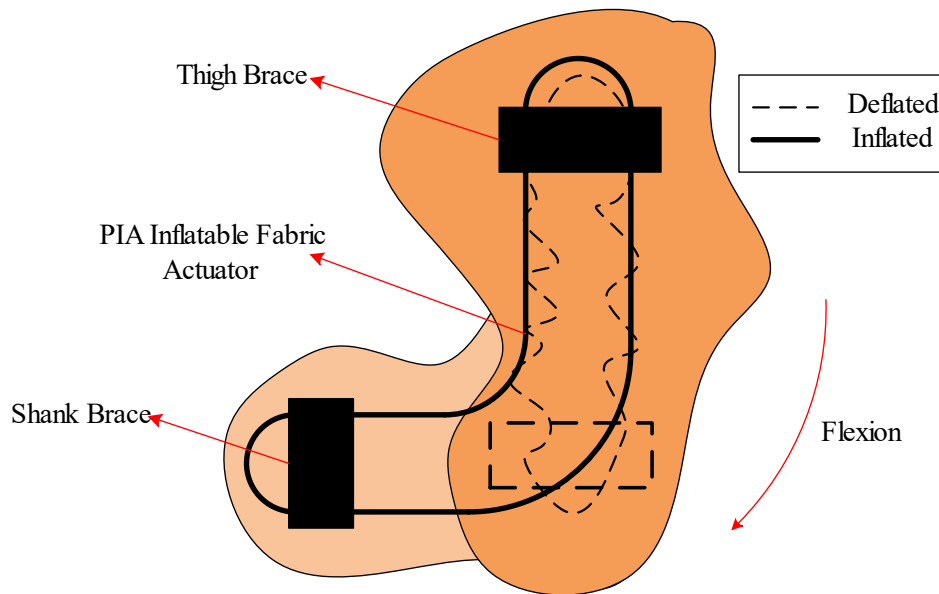


Figure 2.3. Demonstration of the CPIA on the Knee.

To make a decision on which concept is the best, Pugh's method described in (Yoder et al., 2017) has been applied to establish a decision matrix and define the decision criteria. Biomechanically, there are many factors that should be considered to develop a pneumatic

actuator capable of doing knee flexion. For example, knee flexion happens in a short period of time during the swing phase which means that the actuator should have inflation and deflation response within that period. Also, the actuator should deliver the torque anthropomorphically to the human subject to achieve comfortability. In addition to the biomechanical factors, there are other factors like manufacturability and size compactness that are considered important as well. Therefore, the decision criteria are defined as follows:

- Inflation and deflation duration
- Anthropomorphism
- Manufacturability

The 3 criteria have been given weights according to their importance. The Inflation and deflation duration has been given a weight of 50 as it is directly related to the biomechanical requirements of the knee joint. The anthropomorphism criterion has been given the second higher weight of 30 as it is directly associated with the interaction with human. Nevertheless, the lowest weighted criterion of 20 is the manufacturability as it does not directly affect the either the biomechanical or the human interaction. For their knowledge and experience in the field of soft robotics, a decision matrix has been established and given to each member of the soft robotics team of the Robotics and Intelligent Systems Laboratory at Arizona State University to fill. The total scores given by the participants are summarized in Table 2.1. The participants' matrices are included in Appendix A.

From the table it can be concluded that the CPIA has the highest number of points and the PAM is the second while the accordion-inspired is the third. The evaluators were asked about their decisions and they have reported valuable feedback that is worth mentioning. For the PAM actuator, evaluators reported that it could have acceptable inflation deflation response as physically it does not require too much tubing and fittings. Similarly, the CPIA has had the same feedback. On the other hand, as the accordion-inspired actuator consists of multiple separated chambers, it would require much more tubing and fittings to inflate and deflate which increases the inflation and deflation duration.

Table 2.1

Decision Matrix to Evaluate the Concepts.

Issue: Choosing a Knee Flexion Actuator		PAM	Accordion-Inspired	CPIA
Inf/Def Duration	50	3	-4	3
Anthropomorphism	30	-1	2	3
Manufacturability	20	1	-4	4
	Total	1	-6	10
	Weighted Total	140	-60	320

For anthropomorphism, the evaluators voted for the CPIA. That is because the CPIA's geometrical features give the flexibility to be designed with a curvature that aligns with the knee's geometrical features and thus interacts with the knee anthropomorphically. For the accordion-inspired actuator, it is challenging to align the actuator with the knee's geometrical features as that requires more complicated manufacturing processes to make the actuator inflate anthropomorphically. The PAM actuator took the worst score in anthropomorphism as its contractile motion results in volume increase laterally which is not ideal for interaction with humans. In addition to that the PAM actuator contracts linearly and cannot be integrated in such a way to align with the knee's geometry.

For manufacturability, the CPIA is the simplest and easiest to manufacture as its manufacturing includes simple heat sealing and fabric sewing processes. On the other hand, the accordion-inspired actuator requires more complicated stitching and heat-sealing processes to manufacture each individual chamber in addition to more complicated stitching to assemble the whole actuator. Also, the PAM actuator is more complicated to manufacture as it requires thorough fabric or thread weaving as well as placement of cylindrical flanges on actuator's ends.

Therefore, the attention has been focused on designing and manufacturing a CPIA actuator that can achieve the knee flexion biomechanical requirements.

2.2. CPIA Description and Principle of Operation

The CPIA consists of an inflatable thin plastic tube made of a thin thermoplastic polyurethane (TPU) with 0.1524 mm thickness (American Polyfilm Inc., Branford, CT), and an outer nylon fabric (Seattle Fabrics. Inc., Seattle, WA) stitched tube as illustrated in

Figure 2.4. A pipe fitting gland is pinched through the polymeric and fabric layer and threaded by mechanical nut to prevent air leak. When deflated, the CPIA acts as a compliant piece of cloth, and when inflated it exhibits passive spring behavior. The stiffness of the actuator is generated by the pressurized air inside. When the pressurized air inside the actuator is subject to a change in volume by buckling the actuator or squeezing it, the pressure inside increases as a response. From the principle of virtual work, described by Eq. (3.1), this change in pressure and volume will result in a work exerted by the actuator to restore it back to its initial equilibrium state.

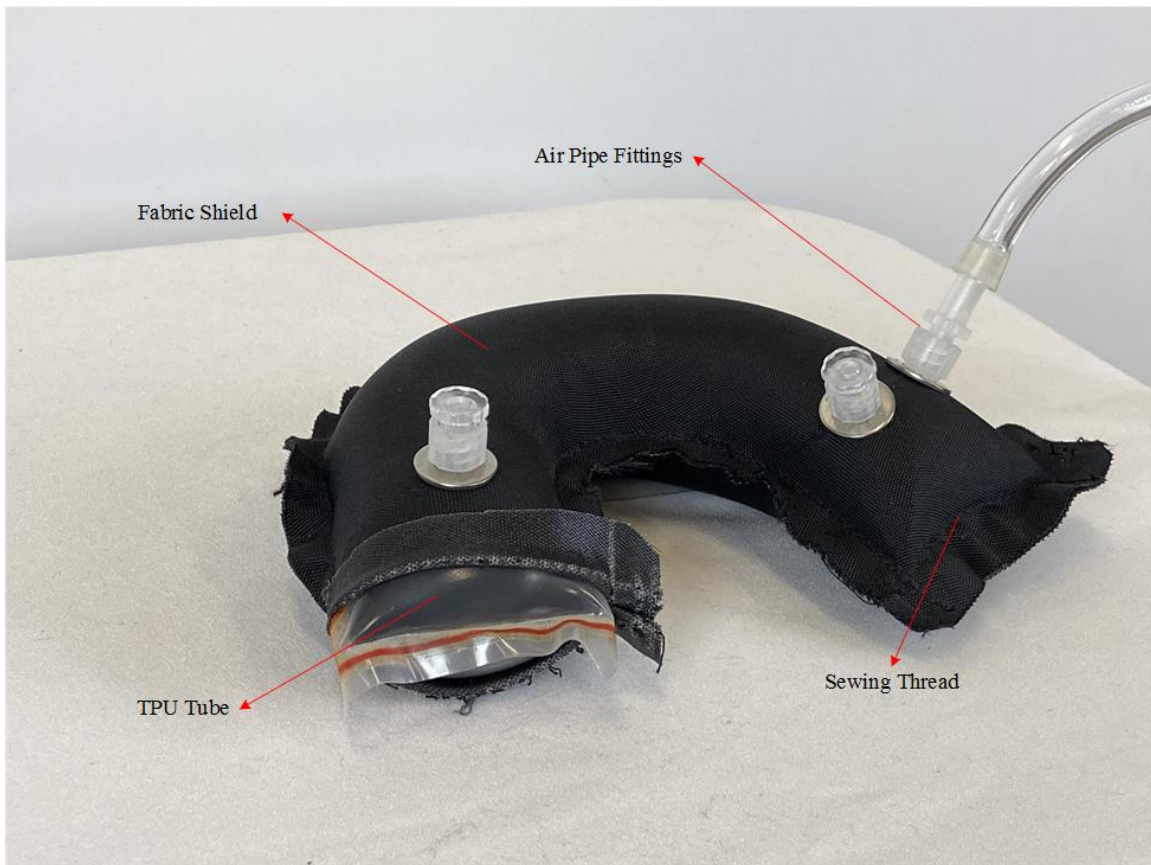


Figure 2.4. CPIA Actuator's Structure.

Understanding the actuator's principle of operation is crucial to customizing the CPIA actuator to generate flexing torque to the knee. As the knee's flexion motion is curvilinear, it is essential for the actuator to generate a torque following this path. Therefore, the actuator has been proposed to have a curved geometry such that it aligns with the knee's geometry when it is flexed. When the knee is extended and the actuator is inflated, the actuator is bent as illustrated in Figure 2.5.

In that state, the actuator's volume is squeezed as if an external force has been applied to transform it from its initial inflated curved equilibrium state to this unstable state. According to the principle of virtual work, the change in volume, folded volume in Figure 2.5, leads to a generation of a resistive torque to bring the actuator back to the initial equilibrium state and thus flexes the knee. To characterize the torque output of the CPIA, a detailed analytical analysis is derived in CHAPTER 3 to mathematically formulate this interaction.

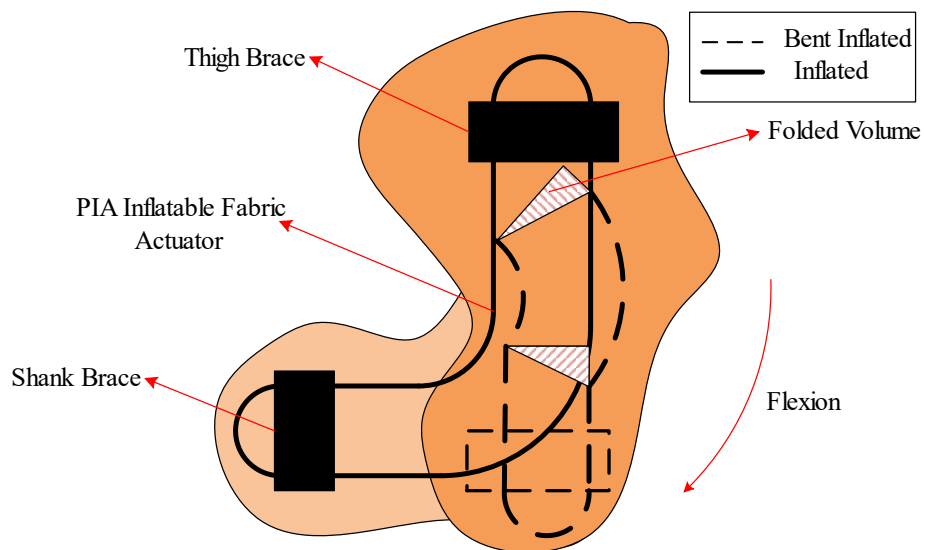


Figure 2.5. CPIA in Inflated Folded State.

2.3. Braces Design

The integration of the actuator to the human is an important factor to ensure torque transfer to knee. To achieve this, a few requirements have been identified as essential to develop a functional and reliable actuator integration to the body. These requirements are listed as follows:

- Adjustability to fit different human subjects,
- Well clamping to the leg that minimizes slipping and torque transfer losses due to the existence of soft tissues underneath,
- Anthropomorphism and prevention of misalignment issues that result in undesired torque generation in the coronal plane,
- Mechanical strength to withstand the resulting stresses.

2.3.1. Fabric Brace

At first, efforts were focused on designing full fabric reinforced braces for both thigh and shank as demonstrated in Figure 2.6. This design did not achieve the aimed requirements; however, the braces have been reinforced by inextensible fabrics.

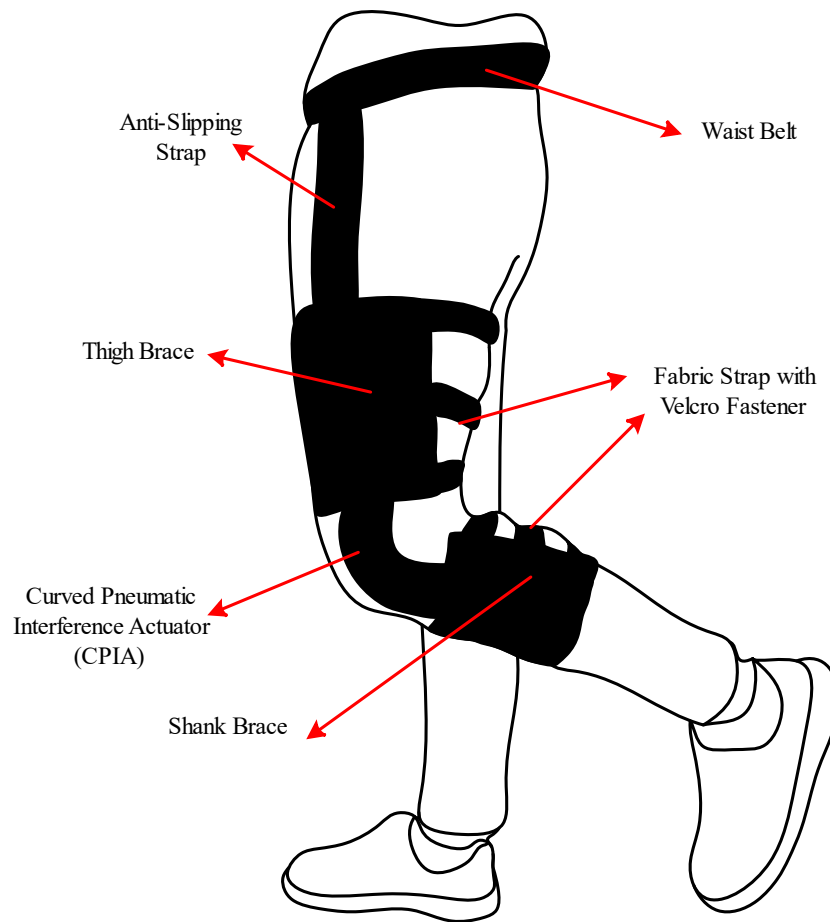


Figure 2.6. Exosuit with Soft Fabric Braces.

This is because the fabric only supports tensile forces while the actuator exerts torsional forces. Therefore, the produced torque of the actuator is wasted in twisting the fabric around the anchoring point rather than being transferred to the joint. In addition to that, to maintain the volume of the actuator as minimum as possible, the fabric braces were placed as near as possible to the knee joint which resulted in a lot of tension exerted on the tendons behind the knee that led to walking difficulty. Moreover, as the actuator must be anchored to the brace such that fabric is stitched at the centerline of the cross-section to

prevent twisting as much as possible, the actuator presses on the adjacent tissues when it is inflated as illustrated in Figure 2.7 which makes the user less comfortable.

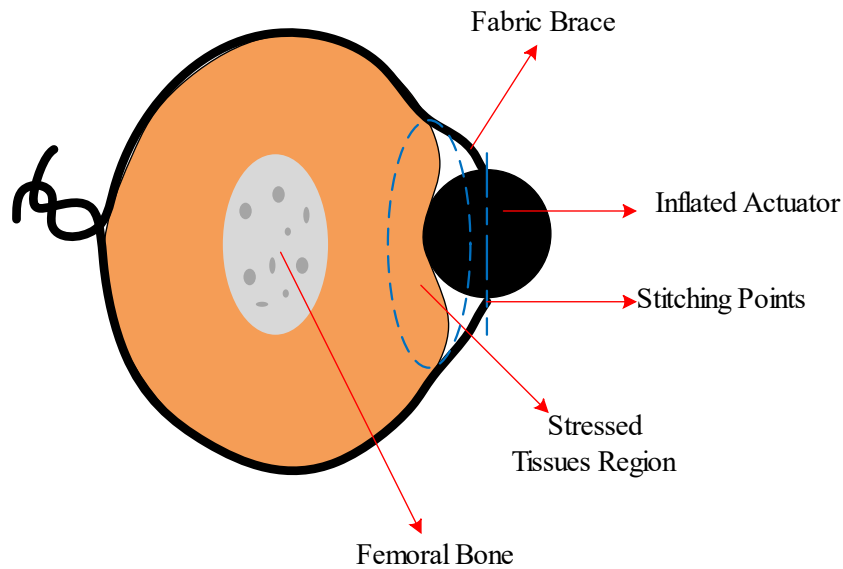


Figure 2.7. Top View of Tissue Stress due to Actuator Inflation with Fabric Braces.

2.3.2. 3D Printed Brace

To address the problems experienced with the soft fabric brace, the focus has been directed to develop a brace that can achieve some rigidity enough for torque transmission. Following the same methodology, the requirements mentioned before in section 2.3 are considered. The brace's concept is based on designing modular 3D printed segments that can be assembled to clamp the leg at the desired anchoring points namely, thigh and shank. As illustrated in Figure 2.8 and Figure 2.9, the brace is designed such that the modular parts are connected by revolute joints to allow rotation that keeps circumferential contact between the brace and the leg as well as allow size adjustability. The closure method

employs reinforced fabric straps with stitched Velcro bands to allow tightness adjustability by applying tension forces at the fabric strap grooves.

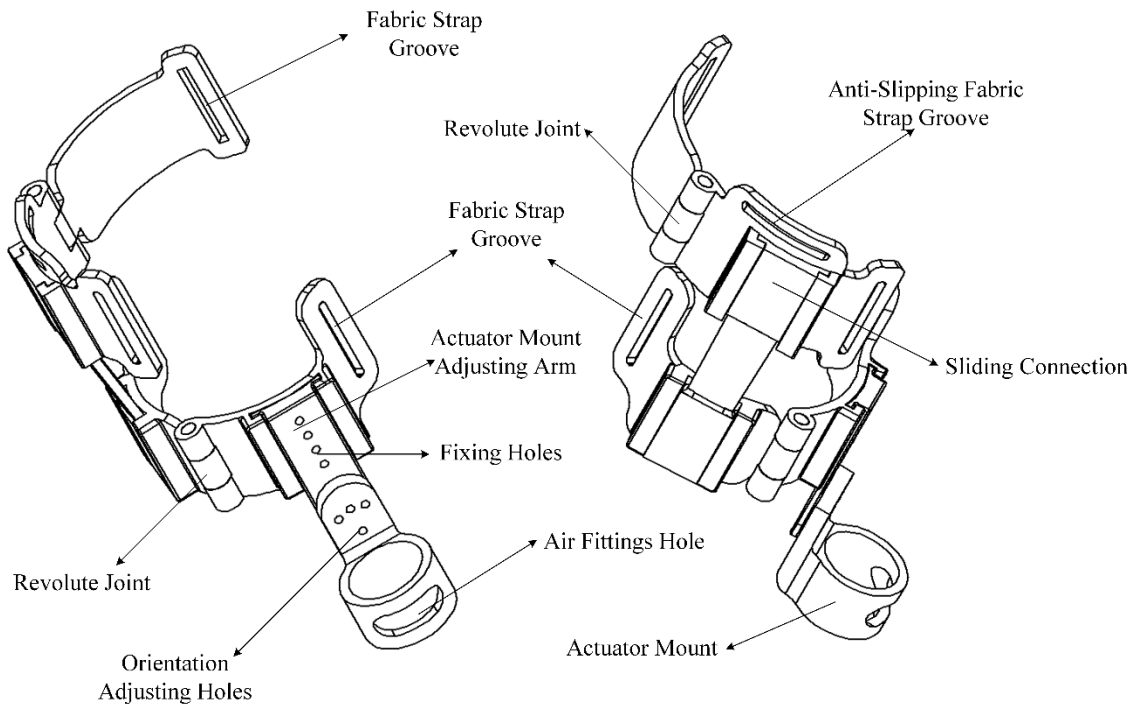


Figure 2.8. Thigh's 3D Printed Modular Brace Drawings.

In addition to that, the actuator's mounts are connected to both thigh and shank by sliding connection that allows the mount to slide up and down to align the actuator's center of curvature with the center of rotation of the of the knee joint. By adjusting the mount, the sliding joint is locked by mechanical fasteners through the fixing holes to hold the mount at the desired position and orientation. The braces have been printed using polylactic acid (PLA) thermoplastic material. Figure 2.11 and Figure 2.12 illustrate the printed braces integrated with the human body and the CPIA in inflated and deflated states.

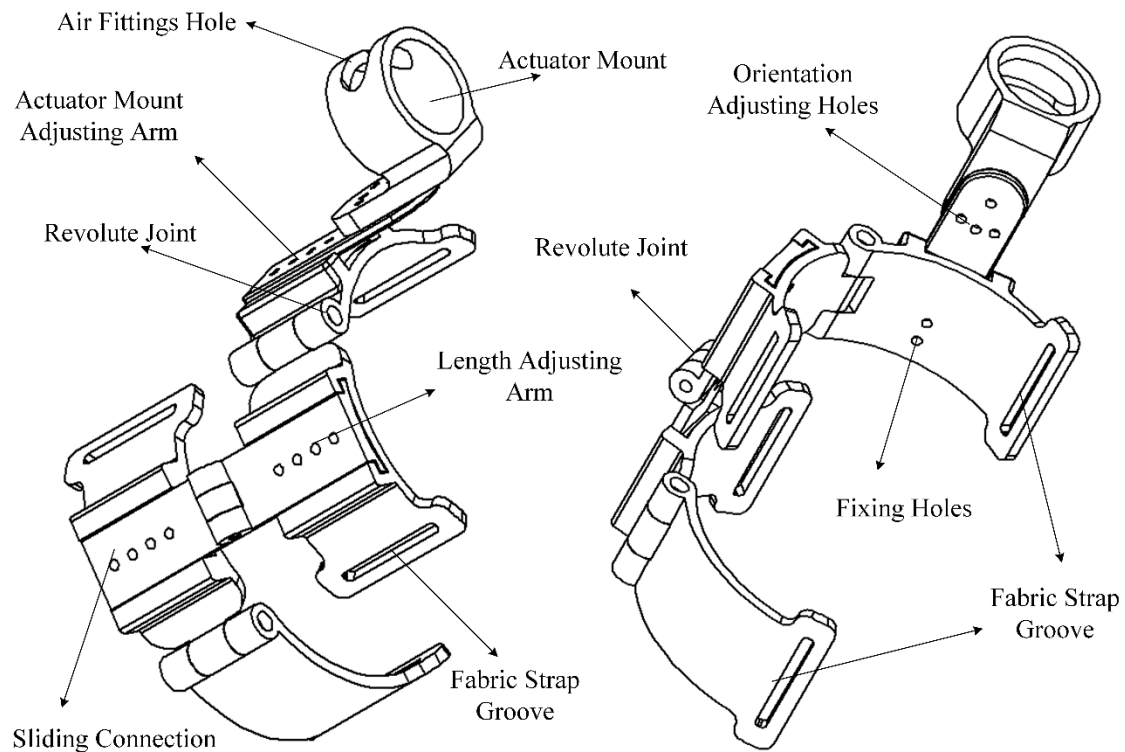


Figure 2.9. Shank's 3D Printed Modular Brace Drawings.

2.4. Final Exosuit

As illustrated in Figure 2.10, the exosuit is integrated to the leg by forming two anchoring regions by the thigh and shank braces. The braces give rigidity that reduces the torque transmission losses as well as providing well clamping to the leg. To avoid slipping of the braces, fabric straps and buckles have been used to design an anti-slipping connection that anchors the thigh brace to the waist through a waist belt. Moreover, to accommodate subjects with different heights, the thigh brace is connected to the waist belt by buckle connection to lengthen and shorten the fabric strap according to the subject's height. Figure 2.11 and Figure 2.12 show front views of the real integration of the exosuit in deflated and inflated states consequently.

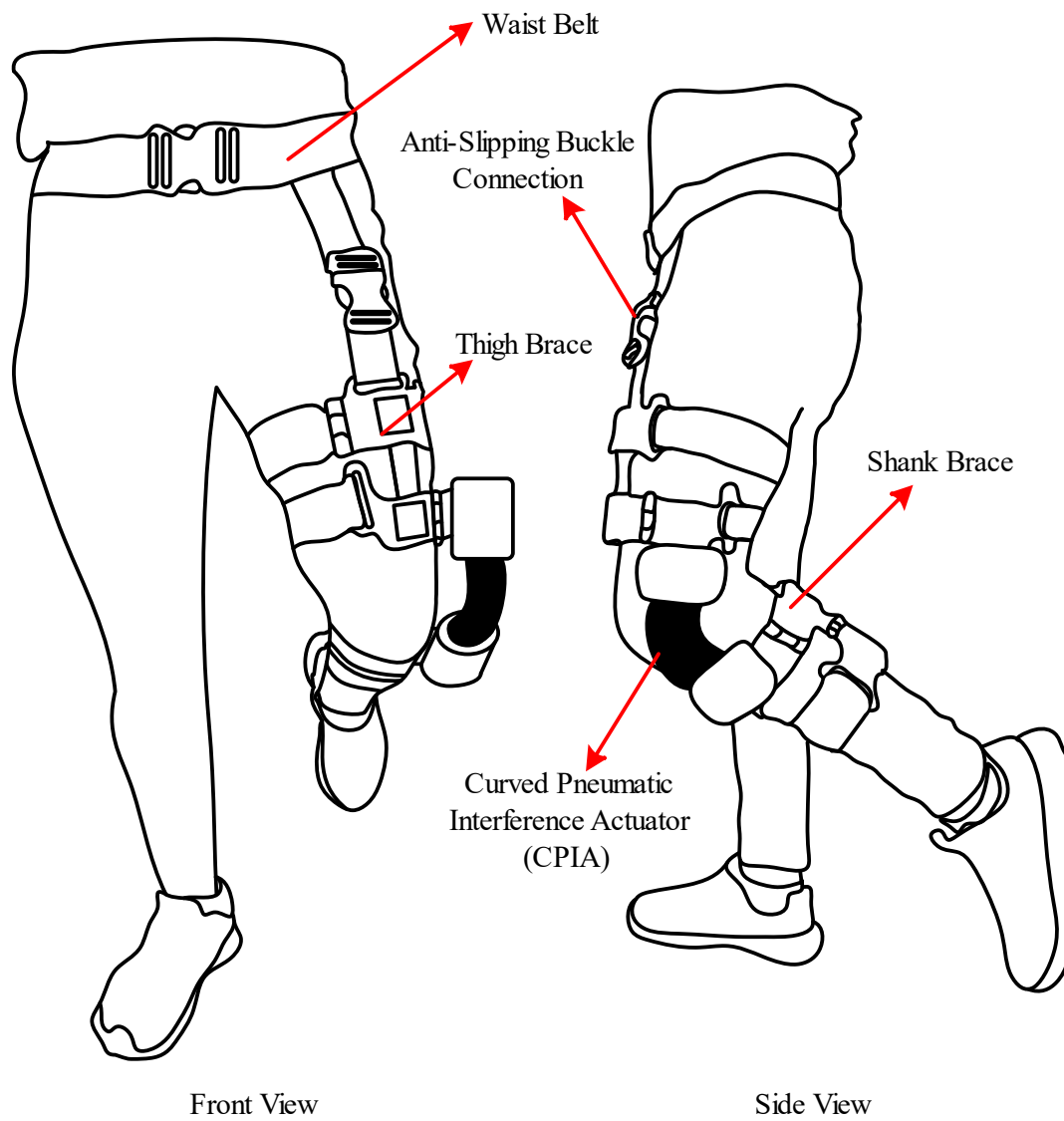


Figure 2.10. Exosuit Demonstration with 3D Printed Braces.



Figure 2.11. Front View of Real Integration of the Exosuit In Deflated State.



Figure 2.12. Front View of the Real Integration of the Exosuit in Inflated State.

CHAPTER 3

CHARACTERIZATION

3.1. Knee Joint Biomechanical Requirements

To determine the amount of torque needed to assist the knee joint, the torque and angle profiles during the gait cycle should be understood. According to (Zhang et al., 2020), there are two flexion and two extension angle peaks, two of them happen in the stance phase and the other two happen in the swing phase. Similarly, for the torque, there are two flexion peaks and two extension peaks. All the torque peaks occur in the stance phase except one flexion peak that takes place in the swing phase. As the interest is to provide flexion assistance during the swing phase, quantifying the flexion torque during that period is essential to the exosuit development. Table 3.1 summarizes the values of flexion angle and torques at relevant gait events during the swing phase.

Table 3.1

Summary of Biomechanical Knee Flexion Torque Requirements.

Study	Subjects	Mean Weight \pm SD (kg)	Speed (m/s)	Max Flex Angle	Specific Peak Flexion torque (Nm/kg)
(Collins et al., 2015)	9	77.4 \pm 9.2	1.25	61°	0.388
(Shamaei et al., 2014)	3	68.6 \pm 2.2	1.25	69°	0.379
(Ding et al., 2017)	8	78.5 \pm 9.9	1.25	75°	0.420
(Mooney & Herr, 2016)	6	89 \pm 8	1.4	78°	0.378
(Van Dijk & Van Der Kooij, 2014)	8	75.1 \pm 6.5	1.11	-	0.320
(Shemmell et al., 2007)	28	66.3	1.32	-	0.3

As the aim is to assist the knee flexion by designing the exosuit to generate torque as a percentage of the peak flexion torque, the peak values listed in Table 3.1 are needed to be averaged. To find the average, first the weight is averaged such that the mean weight of each study is multiplied by the number of subjects of the same study and then taking the sum of this quantity to all studies and finally divide by the total number of subjects for all studies. Similarly, the specific peak flexion torque has been averaged. By multiplying the resulting weight and specific peak flexion torque, the resulting averaged peak torque of all studies is 29 N.m. Therefore, to provide 7.5% assistance of the peak torque during knee flexion in the swing phase, the exosuit needs to be designed to deliver a peak torque of 2 Nm approximately during that assistance period.

At first, an experimental approach has been followed to develop an actuator capable of delivering the required amount of torque. Several CPIAs have been manufactured and their torque has been measured experimentally. The experimental testing setup and methodology are the same as these used in the experimental model discussed in section 3.2. In this experiment the pressure has remained constant, and the flexion angle changed from 0° to 90° while recording the torque output torque at each flexion angle. As the knee flexes from 0° to a maximum of 70° which is the average of the max flexion angles in Table 3.1, the objective is to develop an actuator that can deliver a maximum torque of 2 Nm in the target flexion angles range which is 0° to 70°.

After testing several actuators, it has been found that an actuator with a 4 cm diameter and a 60° curvature angle at 20 psi pressure, as shown in Figure 3.1, can produce

a maximum of 3 Nm torque at 0° when the knee is fully extended and decreases to 1.2 Nm at 70° . This actuator looks a good candidate to deliver the target torque such that it delivers an average torque of 2.2 Nm approximately during the assistance period from 0° to 70° . Nevertheless, to automate the process of the actuator design, an analytical model is derived in the subsequent sections and experimentally validated to deduce a validated mathematical formula that can precisely predict the torque output of the CPIA.

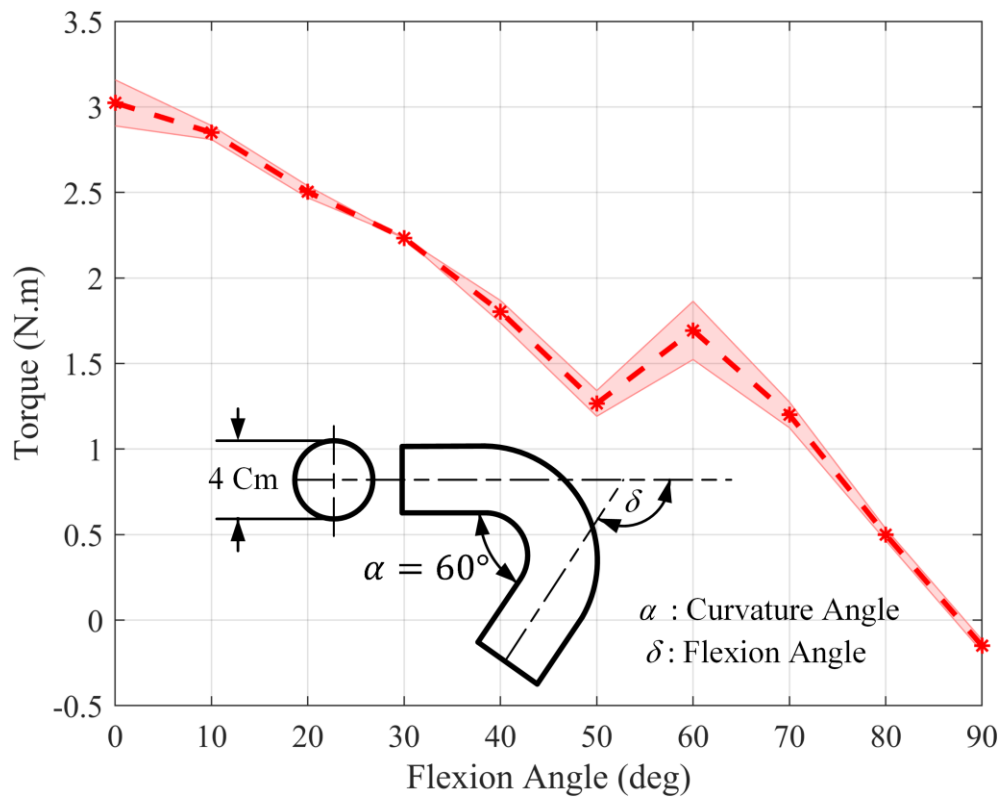


Figure 3.1 Experimental Torque Values of the Candidate CPIA at 20 psi.

3.2. Torque Characterization

The objective of the exosuit is to deliver the required amount torque to the knee joint. To achieve that, the CPIA should be designed to generate the torque requirements.

In this section, a torque characterization analytical model to predict the CPIA output torque has been derived and validated experimentally.

3.2.1. Analytical Model

An inflated fabric actuator produces a resistive torque if it is loaded by an external loading that makes it buckle. This resistive torque happens as a response to the change in the internal volume and pressure of the pressurized fluid inside the actuator. The actuator's volume decreases because the actuator physically folds at the buckling point to accommodate the external load while the internal pressure increases because the volume decreases. This behavior is like a torsional spring element which stiffness forms resistance to external loads by generating a resistive torque in the opposite direction. To model this behavior, the principle of virtual work is applied as follows,

$$\tau \times d\theta = P \times dV(\theta) \quad (3.1)$$

where, τ is the torque produced by the actuator, θ is the buckling angle, P is the pressure applied and $V(\theta)$ is the actuator's volume as a function of the buckling angle.

To precisely predict the torque output, the change in actuator's volume is needed to be calculated according to the actual change in volume that happens experimentally. In (Nesler et al., 2018), the authors derived closed form analytical formulas to evaluate the torque and work produced by the PIA. They also experimentally validated the derived models for two type of actuators at different pressures and deflection angles. The results showed that the proposed analytical models successfully predict the maximum torque and agree with the pressure volume relationship. Nevertheless, unlike the analysis derived in (Nesler et al., 2018), our experimental observations, illustrated in Figure 3.2, showed that,

under loading, the actuator buckles such that the upper side under tension smoothly bends to form a curvature, whereas the lower side under compression self-intersects and forms a sharp change in the actuator profile.



Figure 3.2. PIA in Folded State.

This observation means that (Nesler et al., 2018) overestimated the actual change in volume at buckling angle θ such that in their analysis the volume has been calculated to be the red hatched area indicated in Figure 3.3(a). On the other hand, in our analysis, the change in volume at a given buckling angle θ is approximated as the red hatched area in Figure 3.3(b).

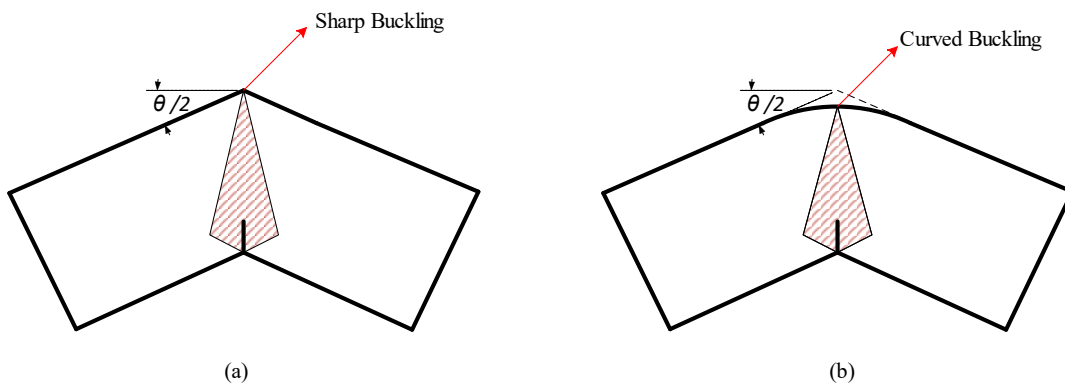


Figure 3.3. (a) (Nesler et al., 2018), (b) Experimental Observation.

From the trigonometry in Figure 3.4, the volume of the actuator $V(\theta)$ at any given bending angle is evaluated by Eq. (3.2).

$$V(\theta) = \pi D^2 L - \frac{\pi}{4} C^2 h \quad (3.2)$$

Where, D is the actuator's diameter, L is the length of the actuator.

For simplicity, the curvature mqn in Figure 3.4 is assumed to be circular. As \overline{ms} and \overline{ns} are tangents to the curvature mqn , and $\overline{om} \perp \overline{ms}$, $\overline{on} \perp \overline{ns}$, therefore, point o is the center of the curvature mqn and \overline{om} , \overline{on} and \overline{os} are radii to that curvature. Hence, the variable C can be calculated by applying the law of cosine to triangle owq as follows,

$$C = \sqrt{D^2 + (h)^2 - 2D^2 \tan\left(\frac{\theta}{2}\right) \cos(\beta)} \quad (3.3)$$

where $\beta = \frac{\pi}{2} - \frac{\theta}{2}$, and $h = D \tan\left(\frac{\theta}{2}\right)$.

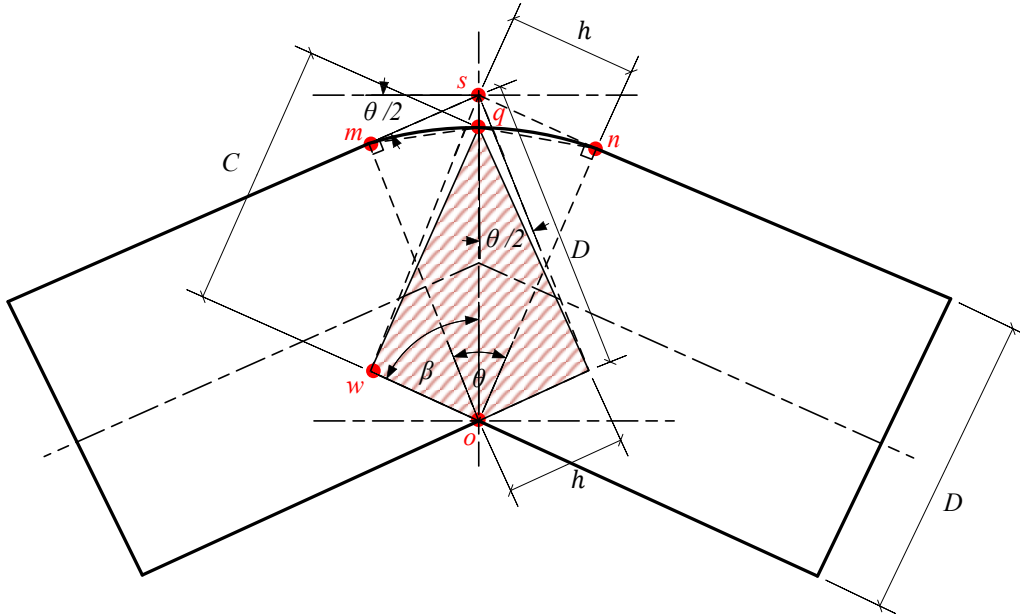


Figure 3.4. Free Body Diagram of the PIA in Folded State.

Hence, From Eq. (3.1), Eq. (3.2) and Eq. (3.3) the output torque can be estimated by evaluating the following equation,

$$\tau = P \frac{dV(\theta)}{d\theta} \quad (3.4)$$

By finding the derivative of the actuator's volume with respect to the buckling angle θ , the torque formula reduces to Eq. (3.5).

$$\tau = -\frac{\pi D^3 P}{8 \cos^4\left(\frac{\theta}{2}\right)} \left[2 \cos^3\left(\frac{\theta}{2}\right) - 2 \cos^2\left(\frac{\theta}{2}\right) - 4 \cos\left(\frac{\theta}{2}\right) + 2 \cos^5\left(\frac{\theta}{2}\right) + 3 \right] \quad (3.5)$$

To apply Eq. (3.5) on the CPIA, the relationship between the buckling angle and the flexion angle should be well-defined. As illustrated in Figure 3.5, when the CPIA buckles, it forms two equal folds indicated by the red hatched triangular areas. Each of these folds is formed at a buckling angle \emptyset . From the trigonometry, this angle is equal to the difference between the flexion angle δ and the actuator's curvature angle α , $\emptyset = \delta - \delta'$. The two folds are equivalent to folds that result from buckling two straight PIAs with the same diameter of the CPIA at the same buckling angle. Nevertheless, the net torque of the CPIA equals only the torque of one PIA because the two folds are formed mechanically in series. Hence our analytical model and the analytical model developed by (Nesler et al., 2018) for a CPIA are described by Eq. (3.6) and Eq. (3.7).

$$\tau = -\frac{\pi D^3 P}{8 \cos^4\left(\frac{\phi}{2}\right)} \left[2 \cos^3\left(\frac{\phi}{2}\right) - 2 \cos^2\left(\frac{\phi}{2}\right) - 4 \cos\left(\frac{\phi}{2}\right) \right] \quad (3.6)$$

$$+ 2 \cos^5\left(\frac{\phi}{2}\right) + 3 \left] \right.$$

$$\tau = -\frac{\pi D^3 P}{8} \left[\tan^2\left(\frac{\phi}{2}\right) + 1 \right] \quad (3.7)$$

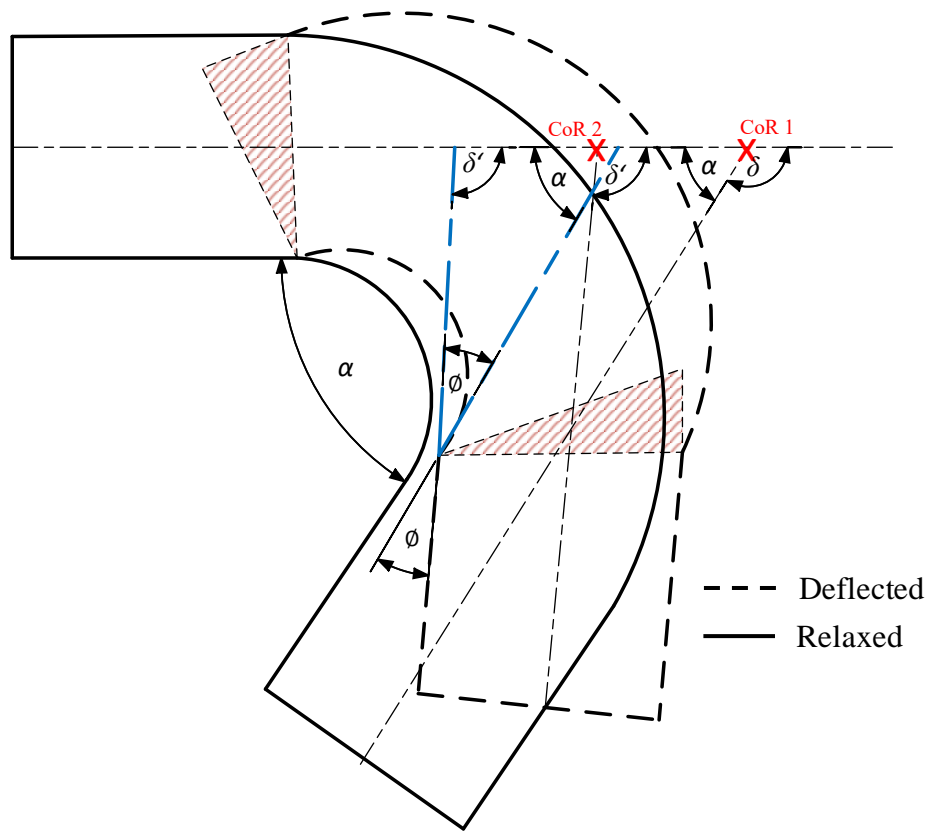


Figure 3.5. Actuator's Trigonometry and Kinematics.

3.2.2. Experimental Model

To validate the analytical model, an experimental setup has been prepared as shown in Figure 3.6. The setup consists of a torque sensor (Forsentek Co, China) that is equipped

with two aluminum arms to mount the actuator on. The actuator has been mounted on the aluminum arms on a manner that is identical to that is intended to be used to mount the actuator on the knee joint.

To perform the testing, an actuator of the dimensions and the geometry shown in Figure 3.1 has been manufactured. The actuator has been tested in a setup that is analogous to the knee joint structure. The two aluminum arms are connected by a revolute joint to mimic the thigh and shank connection of the knee joint. The actuator has been tested at different pressures and flexion angles.

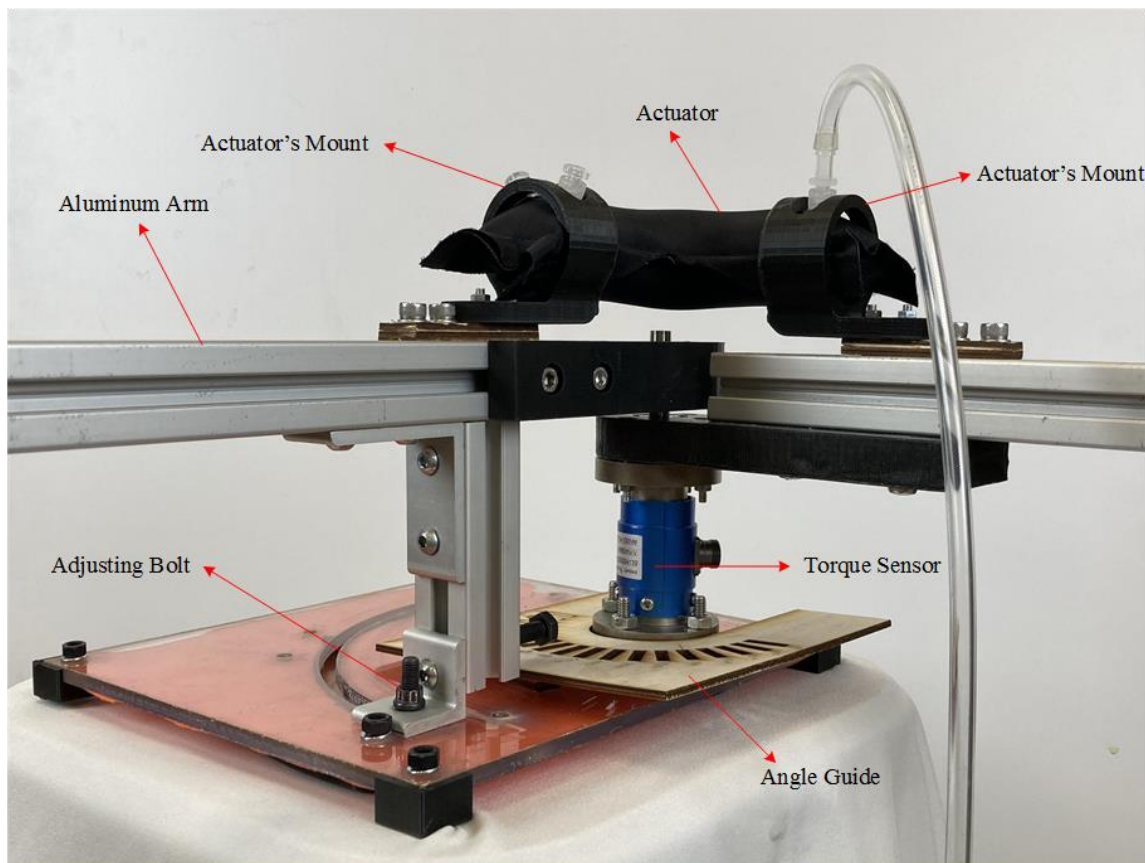


Figure 3.6. Experimental Test Rig.

During the experiment, the pressure range has been varied from 0 psi to 35 psi in increments of 5 psi. As the actuator is designed with a 60° curvature angle, it was expected that it could generate torque at flexion angles below 120°. Nevertheless, when it was tested, it started to produce torque below 90° flexion angle. That is because above 90° the actuator did not buckle or self-intersect which resulted in no noticeable torque measurements. Therefore, the initial testing position of the actuator has been set at 90° flexion angle, and the flexion angle range has been varied from 0° to 90°. Hence, the buckling angle under these conditions is evaluated as $\phi = 90^\circ - \delta'$. To adjust the angle change during the experiment, an angle guide has been used to label the incremental change of the flexion angle required which is 10°. At each flexion angle the torque values have been recorded while the pressure changes from 0 to 35 psi. This procedure has been repeated 3 times at every flexion angle and the averaged torque values of the 3 trials have been computed to be the final torque value.

3.2.3. Torque-Pressure Results and Discussion

In this section, the torque variation with pressure change at different angles is investigated. Experimental values are compared along with results from Eq. (3.6) and Eq. (3.7). For simplicity, we will call the analytical model described by Eq. (3.6) as analytical model I and the other analytical model given by Eq. (3.7) as analytical model II. The results are summarized in figures from Figure 3.7 to Figure 3.16. For readability, the negative sign in Eq. (3.6) and Eq. (3.7) has been eliminated.

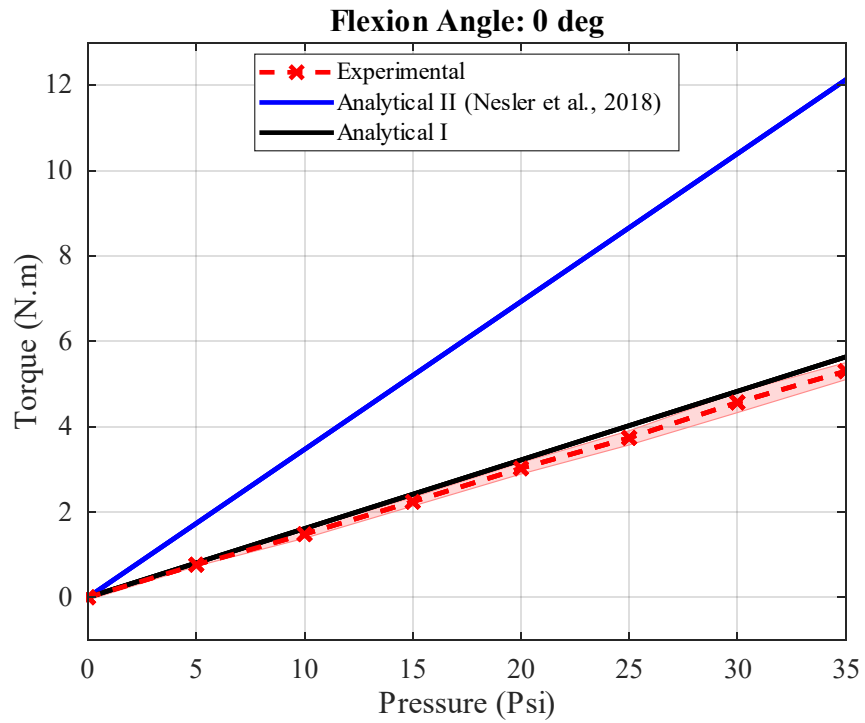


Figure 3.7. Torque Characterization at 0° Flexion Angle.

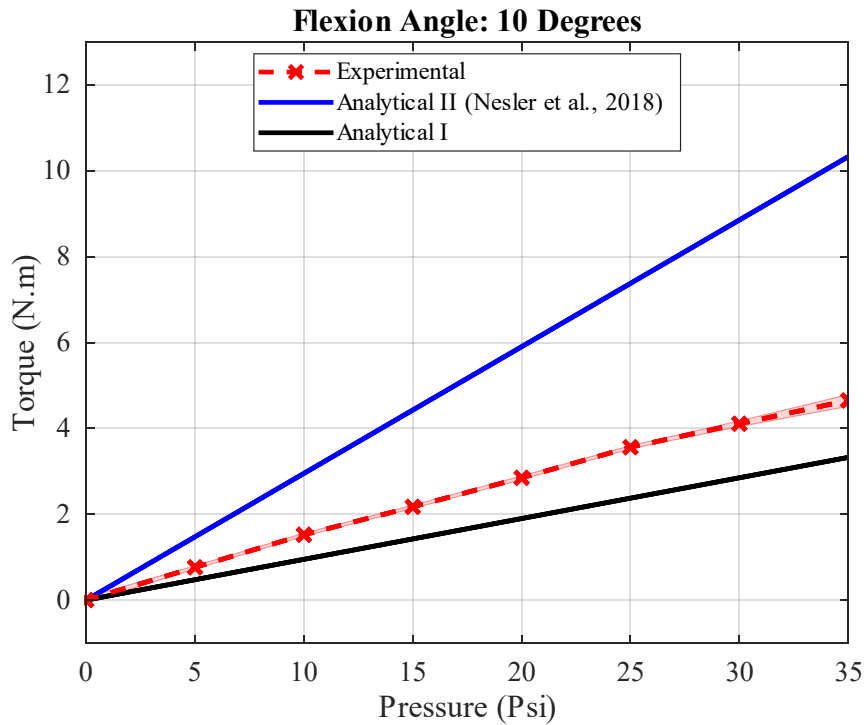


Figure 3.8. Torque Characterization at 10° Flexion Angle.

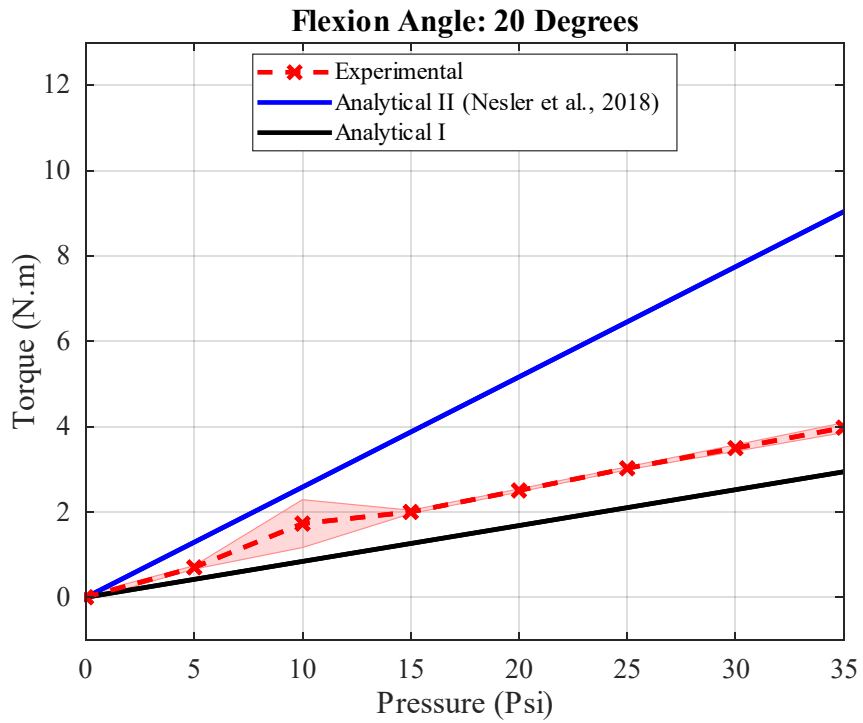


Figure 3.9. Torque Characterization at 20° Flexion Angle.

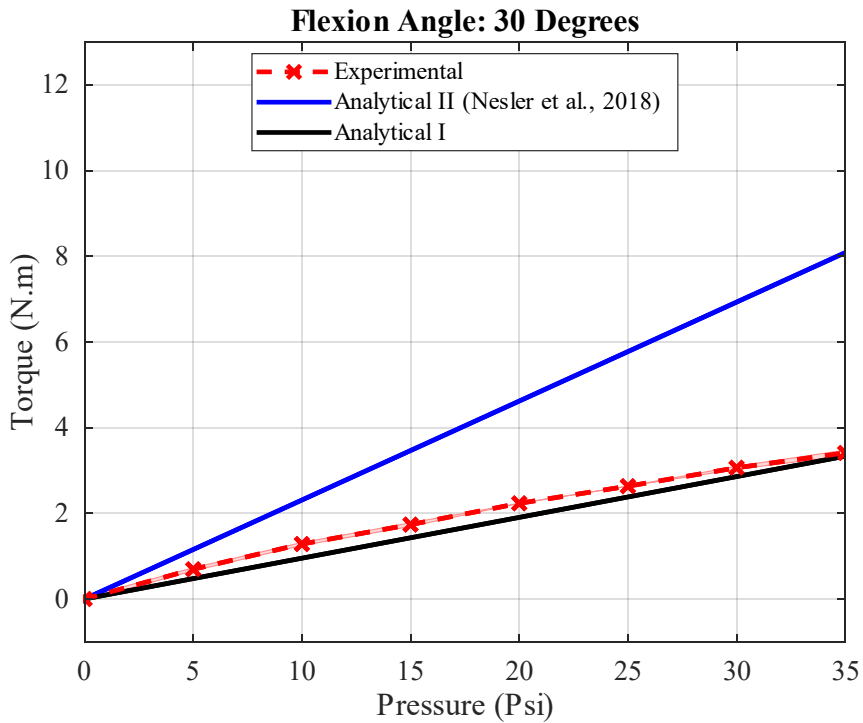


Figure 3.10. Torque Characterization at 30° Flexion Angle.

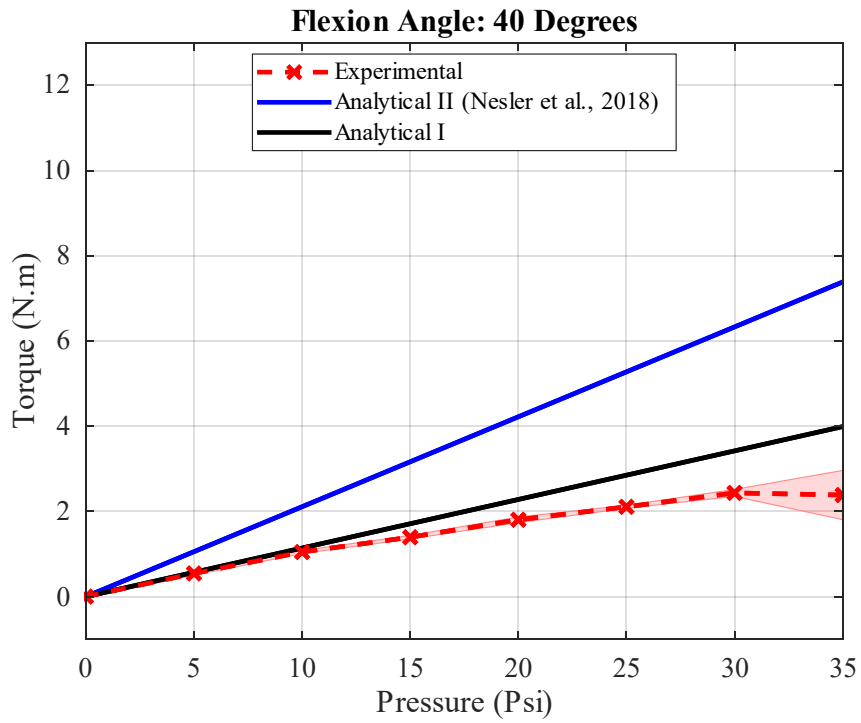


Figure 3.11. Torque Characterization at 40° Flexion Angle.

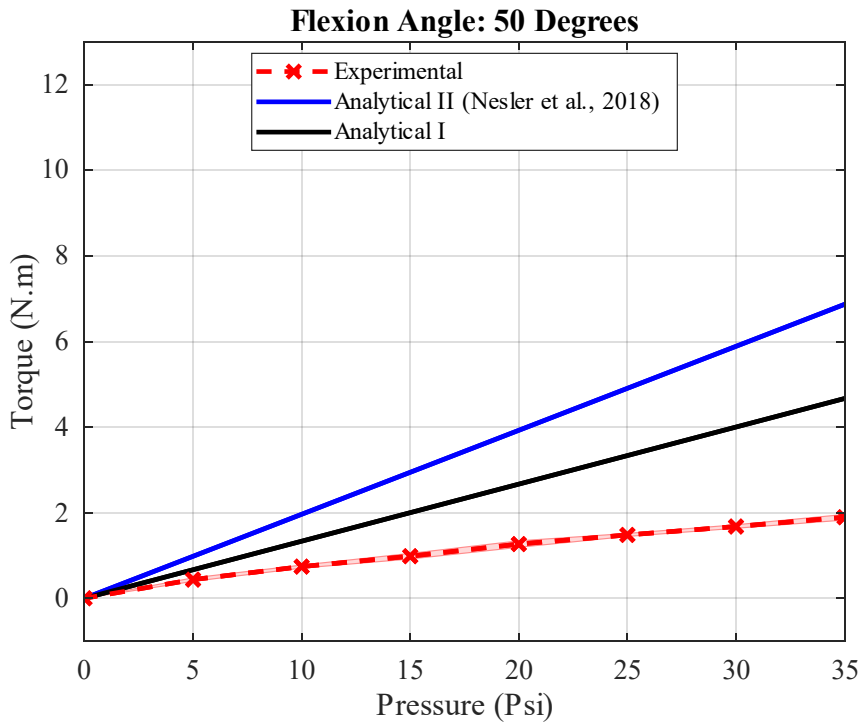


Figure 3.12. Torque Characterization at 50° Flexion Angle.

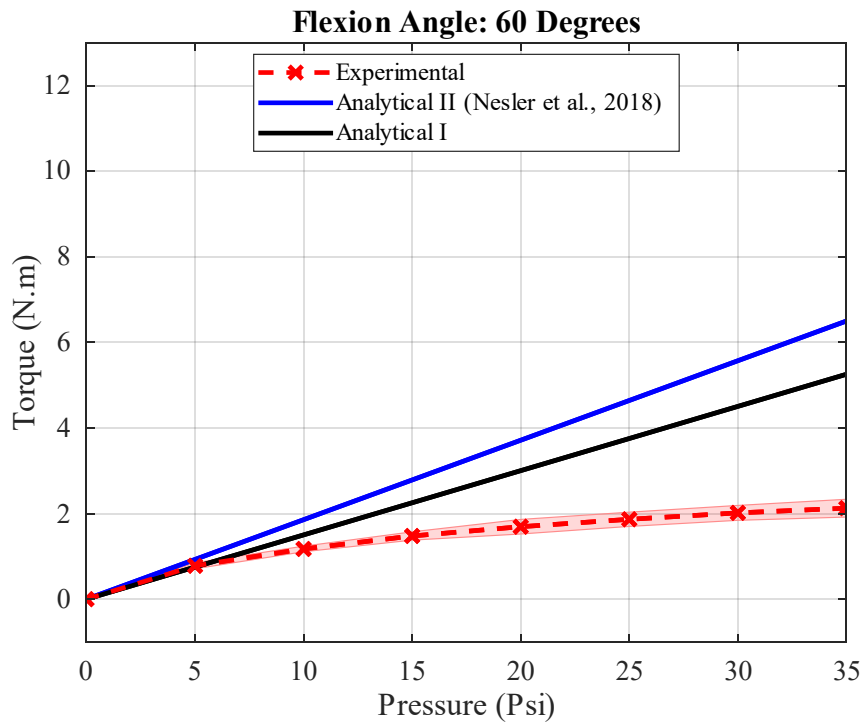


Figure 3.13. Torque Characterization at 60° Flexion Angle.

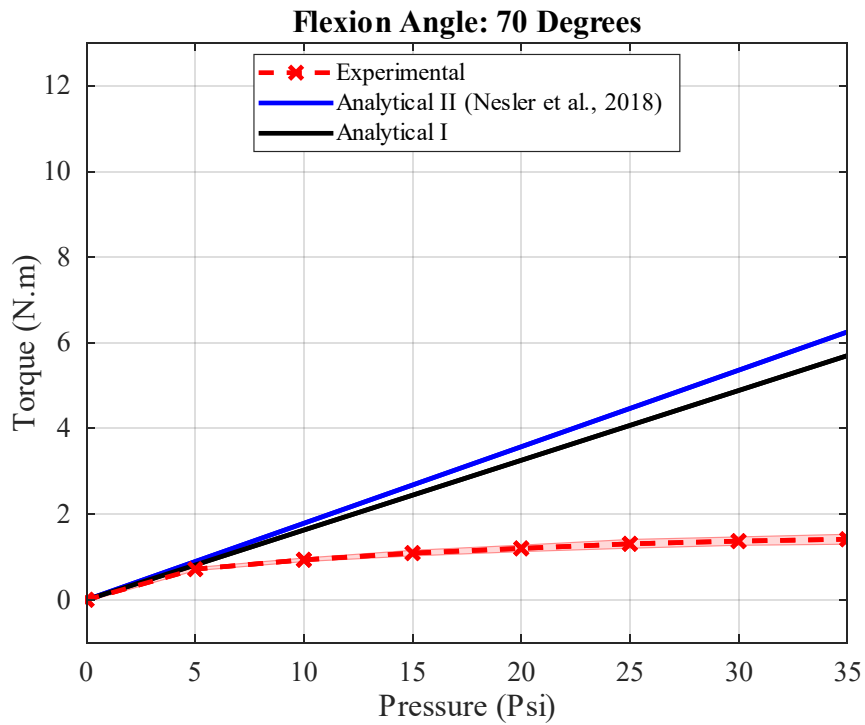


Figure 3.14. Torque Characterization at 70° Flexion Angle.

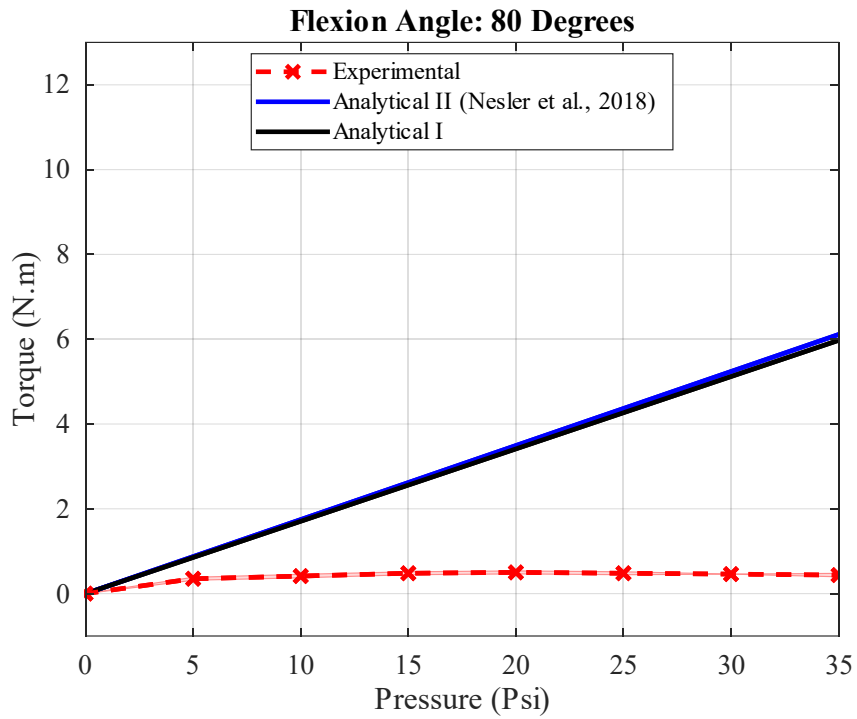


Figure 3.15. Torque Characterization at 80° Flexion Angle.

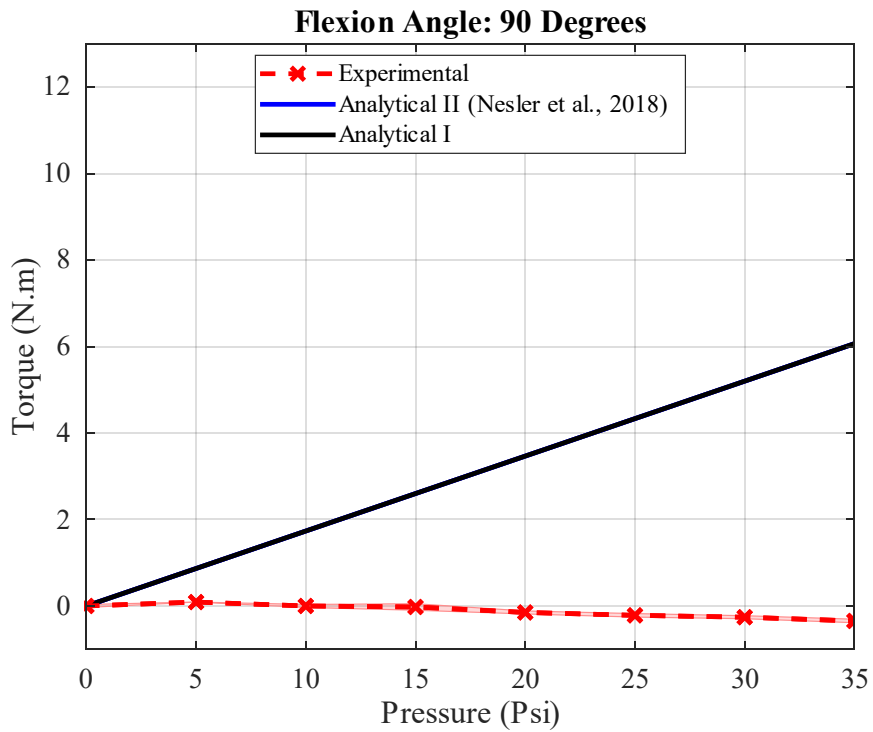


Figure 3.16. Torque Characterization at 90° Flexion Angle.

It is noticed that, although the actuator has been manufactured to have a curvature angle of 60° , it didn't buckle when deflected until it reached a curvature angle of 90° . That's because in this angle range the actuator shows a shearing behavior in which the fabric extensibility allows relative motion among the fabric threads that results in a shearing behavior. At a critical angle, which is 90° curvature angle in this case, the actuator enters a different regime in which it creases, and buckles and the fabric layer tends to self-intersect rather than shearing. A similar finding has been reported by (O'Neill et al., 2021). This also may be resulted from manufacturing issues like misaligned heat sealing and stitching. Another reason could also be that the stitching thread pattern is extensible to some capacity which gives the actuator the flexibility to be extended beyond the designed curvature angle when it is pressurized.

The results showed that analytical model I predicted the experimental values more precise than analytical model II at all flexion angles and pressures tested. It is interestingly noticed that at 0° and 30° flexion angles the analytical model I showed the most precise prediction. The maximum error noticed between the analytical model I and the experimental values at 30° is $\sim 31\%$ of the experimental value at 5 psi, while the minimum error is $\sim 2\%$ of the experimental value at 35 psi. At 0° the maximum error observed is $\sim 8.8\%$ of the experimental value at 15 psi while the minimum error is $\sim 5.4\%$ of the experimental value at 10 psi.

As noticed in figures from Figure 3.13 to Figure 3.16, the experimental values at flexion angles equal or bigger than 60° diverged significantly from the analytical models. That may have resulted because the actuator has a curved geometry and is manufactured

from a fabric woven material which is not fully inextensible, thus the actuator bends rather than buckles at high flexion angles as indicated in figures from Figure 3.25 to Figure 3.28. This behavior could have also happened as a result of the shear that happens in the fabric material such that it stretches laterally which delays the formation of the crease and fold, a similar observation has been found by (O'Neill et al., 2021). That could be the reason for that divergence because the analytical models are based on modeling the torque as a function of the change in the actuator's volume due to buckling. When the actuator bends rather than buckles, the analytical models fail to predict the torque because the actuator does not fold and the change in volume is no longer governed by the equations derived in both analytical models.

In addition to that, at 90° flexion angle it is observed that the actuator experimental values dropped unexpectedly to have negative values such that the actuator is generating torque in the opposite direction. The experimental observations showed that this happens because the actuator forms a fold in the inner curved region as indicated in Figure 3.28. These folds happen because the actuator is fixed such that its ends' displacement is prevented. This fixation method makes the actuator be squeezed as shown in Figure 3.28 because of the misalignment between the center of rotation of the aluminum arms of the experimental test rig and the center of rotation of the actuator. This misalignment takes place because the aluminum arms have a permanent center of rotation (CoR) as they are connected by a revolute joint while the actuator has a CoR that varies with the flexion angle as demonstrated in Figure 3.5.

Furthermore, at 90° flexion angle, it is also noticed that analytical models I and II are identical and the torque output is equal to $\tau = \frac{\pi D^3 P}{8}$. This quantity is measurable if the actuator is slightly buckled from its initial position by a small buckling angle. Although the flexion angle is changed in increments of 5° which is quite large not to precisely measure this value, the experimental values diverged significantly from the analytical models at 0° flexion angle. That is because the physical behavior of the actuator is different such that the folds did not form in the expected region illustrated in Figure 3.5 and they rather formed in the inner curved region as indicated in Figure 3.28. Even before the 90° this divergence also existed until approximately 60°. However, the folds did not form in the inner curved region, there were no significant folds noticed at the expected buckling points.

Overall, the results showed that analytical model I is more precisely predicting the torque-pressure relationship than analytical model II at all flexion angles tested. That is because analytical model I is based on modeling the change in volume closer to the experimental observation noticed in Figure 3.2 unlike analytical model II that models the change in volume as illustrated in Figure 3.3(a). Moreover in (Veale et al., 2020) it has been observed that, analytical model II is overestimating the torque output that is to produce an actuator that generates experimental torque equivalent to the analytical values, the actuator diameter should be designed to be larger than that used to calculate the torque analytically. This observation supports our hypothesis on modeling the change in volume as indicated in Figure 3.3(b).

3.2.4. Torque-Angle Results and Discussion

To investigate the torque-angle relationship, the torque values from Eq. (3.6) and Eq. (3.7) are compared to the experimental torque values while the flexion angle changes, and the pressure is constant. The results are demonstrated in figures from Figure 3.18 to Figure 3.24. The results show that analytical model I is more precise in predicting the torque values in the flexion angles range of interest at all the pressure values tested. On the other hand, analytical model II overlooked model I and the experimental values in all the testing conditions investigated. It is also noticed that analytical model I has two points of intersection with the experimental values near 0° and 30° flexion angles at all pressure values tested. That was also noticed in the pressure-torque relationship such that analytical model I showed the most precise prediction at 0° and 30° flexion angles as shown in Figure 3.7 and Figure 3.10.

From 0° to 60° flexion angles, the trend of analytical model I is like the experimental values such that they start at high torque values and decrease to have troughs then increase again. It is also observed that the two troughs happened at different flexion angles such that the analytical trough took place before the experimental trough at all pressures. From definition of buckling and flexion angles, it is known that the buckling angle increases as flexion angle decreases and vice versa. At 90° flexion angle, the buckling angle is 0° and at this value analytical models have the same value. It is interestingly noticed that analytical model I has a decreasing trend as the flexion angle decreases. As shown in Figure 3.17, this is because the folded volume decreases as the buckling angle increases such that V' is smaller than V . The volume decreases because the analytical

model assumes that the actuator is buckled to have a circular curved profile with a constant radius which is equal to the diameter of the actuator as illustrated in Figure 3.4. This assumption forces the folded volume to decrease until a certain buckling and it starts to increase again until around 80° buckling angle which is equivalent to 10° flexion angle. The volume increases again as the buckling angle goes around 80° because the actuator becomes nearly vertical and aligned with the intersection line. At that instant, the change in the folded volume from the increase in dimension h becomes bigger than that results from the decrease in dimension C .

Finally, it is observed that beyond 60° flexion, analytical models I and II diverge from the experimental results. As discussed before, this divergence happens because the actuator acts physically such that it bends rather than buckles as demonstrated in Figure 3.25 to Figure 3.28. As a result of this behavior, the actuator does not self-intersect significantly that the analytical model cannot describe such behavior precisely.

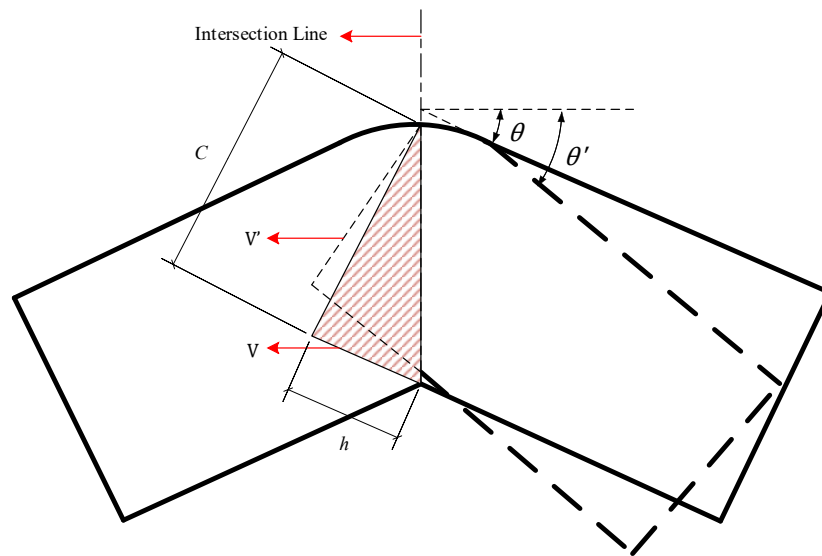


Figure 3.17. Change in folded volume with buckling angle.

3.2.5. Analytical Model Limitations

The analytical model I has shown the potential to predict the torque-pressure and torque-angle relationship of PIAs and CPIAs to a considerable extent. Nevertheless, there are some limitations that made it fail to predict the torque output at some situations. One of these limitations is that the model is based on modeling the torque output just in case the actuator self-intersects as a function in the folded volume. That resulted a divergence between the analytical and experimental values because the actuator bends rather than buckles at higher flexion angles. In addition to that, analytical model I assumes that the actuator buckles to have a circular curved profile with a constant radius which does not physically happen as the radius of the curvature changes as the flexion angle changes. Finally, the analytical model did not account for extensibility that exists in the fabric material and leads to shearing behavior. In future studies, more development is needed to overcome such limitations.

Figure 3.18. Torque-Angle Results at 5 psi.

Figure 3.19. Torque-Angle Results at 10 psi.

Figure 3.20. Torque-Angle Results at 15 psi.

Figure 3.21. Torque-Angle Results at 20 psi.

Figure 3.22. Torque-Angle Results at 25 psi.

Figure 3.23. Torque-Angle Results at 30 psi.

Figure 3.24. Torque-Angle Results at 35 psi.

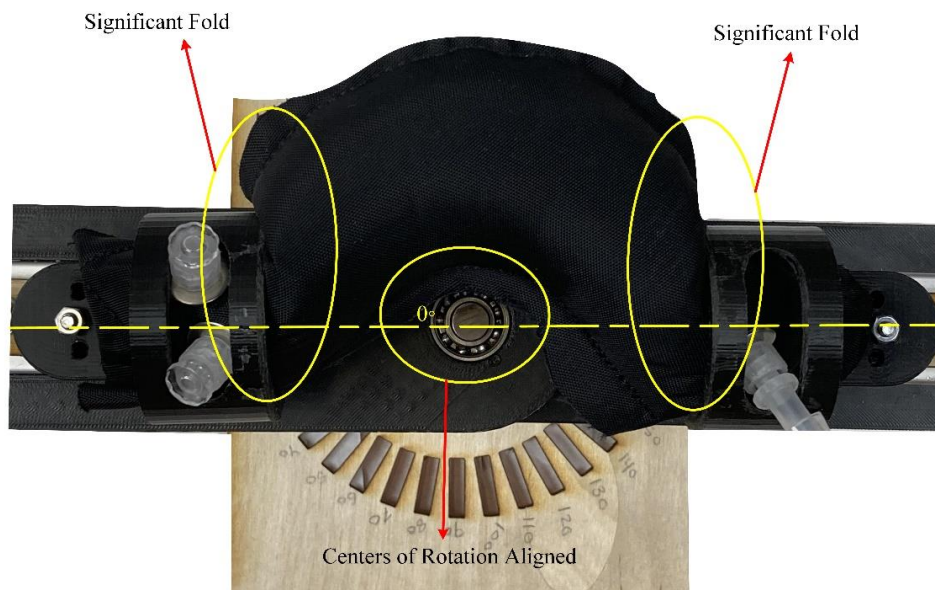


Figure 3.25. Folded CPIA at 0° Flexion Angle.

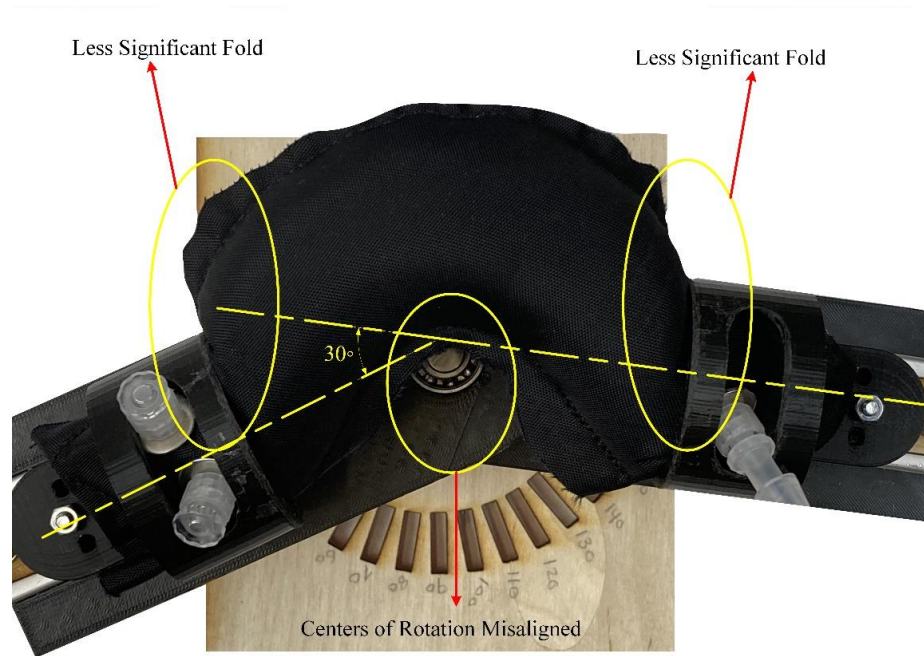


Figure 3.26. Folded CPIA at 30° Flexion Angle.

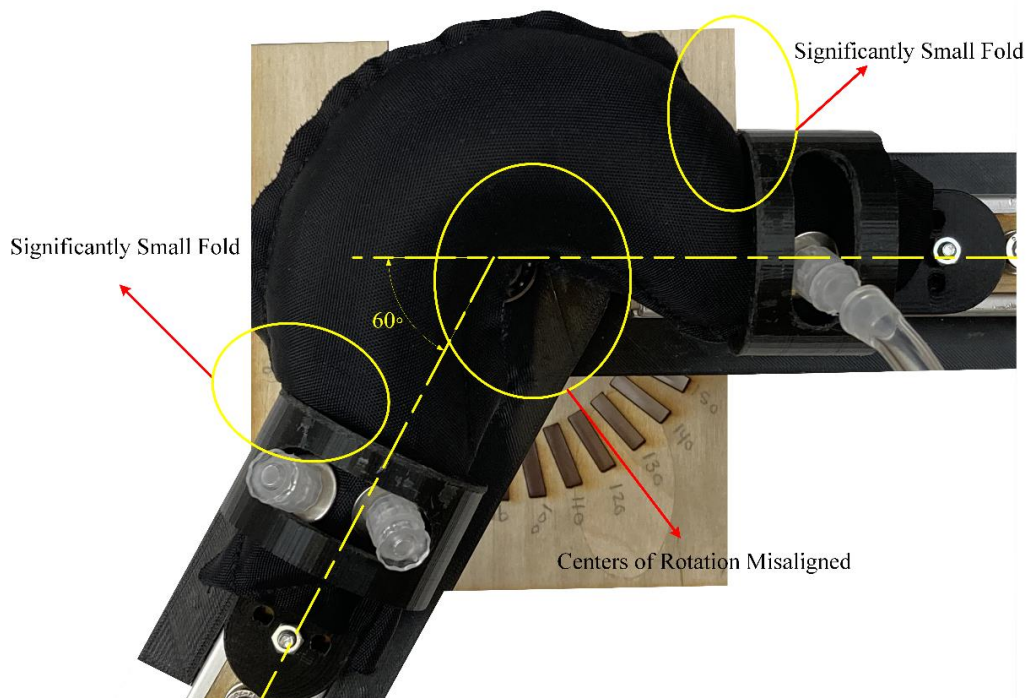


Figure 3.27. Folded CPIA at 60° Flexion Angle.

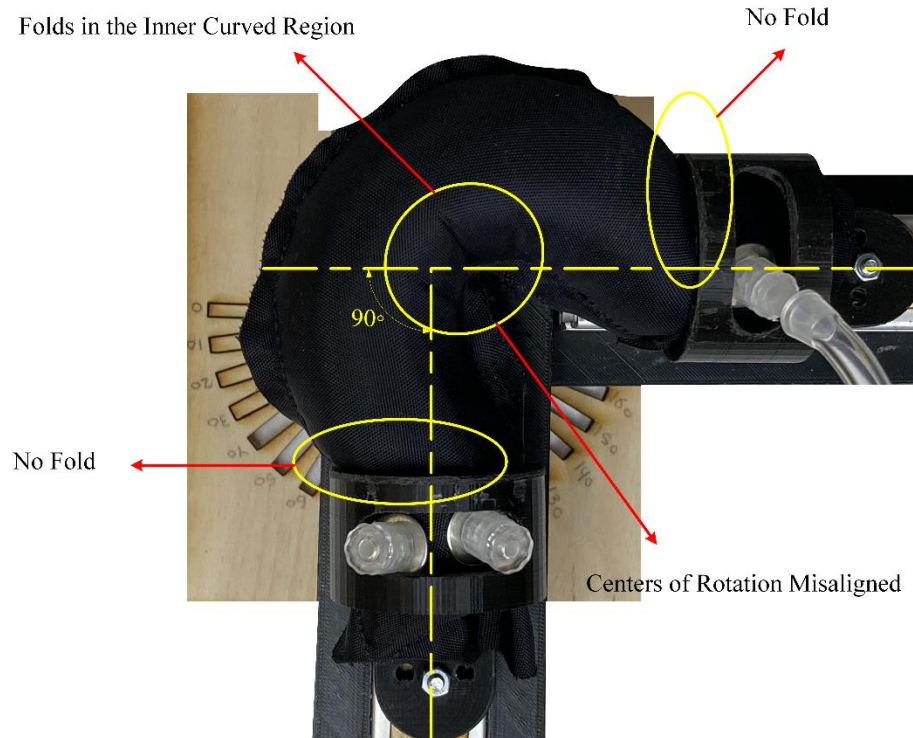


Figure 3.28. Folded CPIA at 90° Flexion Angle.

3.3. Inflation and Deflation Characterization

The inflation/deflation period of the actuator is critical to the actuator's design. This period is dependent on the actuator's volume as well as the piping and fittings. The more the volume and pipe fittings, the more the inflation/deflation period. This is because having a large actuator requires larger amount of air to be compressed into the actuator to be inflated. Also, having more fittings and cross-section reduction in the air manifold builds up resistance to the flow which increases the inflation/deflation period.

The human gait cycle has a bandwidth during which the actuator should operate to properly assist the required joint. An actuator with long inflation/deflation period will result in torque delivery at wrong timing. Therefore, the actuator must be designed carefully to achieve torque delivery within the gait cycle duration. The objective is to design an actuator

that delivers required torque at the correct timing. The knee flexion happens mostly during the swing phase. According to (Murray et al., 1966), the swing phase takes approximately 38 % of the gait cycle with an average duration that ranges from 0.38 to 0.42 s. Hence, the actuator must have inflation/deflation duration which is less than this average term to be able to assist the knee flexion during the swing phase.

To determine the inflation/deflation duration an experimental setup has been prepared to inflate the actuator and then hold the pressure inside for a while and then deflate. This setup is like the hardware setup used to control the exosuit which is discussed in detail in CHAPTER 4, Section 4.2, and illustrated in Figure 4.2. Each inflation, hold and deflation represent an operation cycle out of total 30 operation cycles for the whole experiment. The purpose of the hold duration is to let the pressure inside the actuator enough time to settle around the desired inflation pressure before deflation starts. The pressure time response is then recorded and post processed to calculate the inflation and deflation time intervals. The inflation period has been defined as the time take to inflate the actuator from the initial pressure, at which the actuator acts like a compliant fabric, to the final desired pressure required to generate the required torque. As, discussed before, the actuator produces the required torque at 20 psi, therefore, the desired pressure in this experiment has been set to be 20 psi. Theoretically, the actuator is expected to be 100% compliant when the initial pressure is 0 psi. Nevertheless, the experimental observations showed that the actuator's compliance at 3.5 psi is relatively close to its compliance at 0 psi. Therefore, the initial pressure in the experiment has been set to be 3.5 psi.

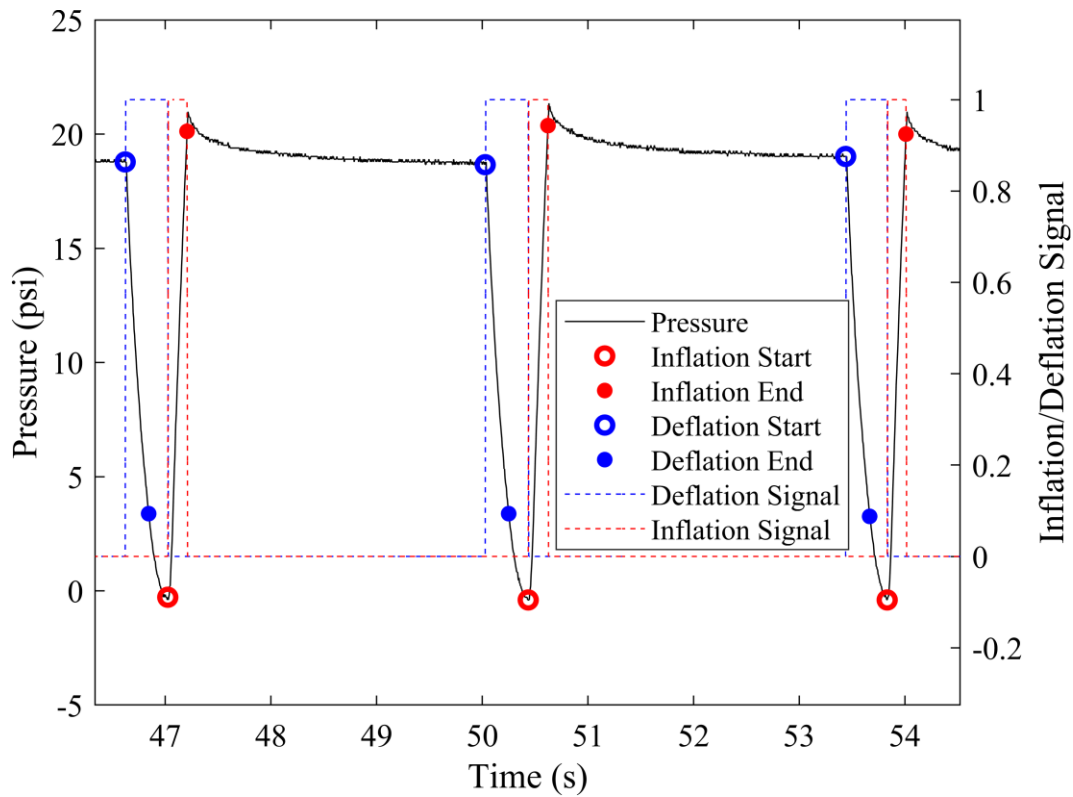


Figure 3.29. Pressure Response of the CPIA.

A sample pressure-time response of a CPIA is illustrated in Figure 3.29 for two cycles. The experiment of the actuator has been performed such that the actuator has experienced 30 operation cycles. The inflation and deflation durations have been calculated for each cycle and averaged. The average inflation and deflation durations are summarized in Table 3.2. The results showed that the deflation time is larger than the inflation time. That because in the experiment, the pressure supply source has been set to be 40 psi such that when the actuator inflates, it is subjected to a differential pressure of approximately 40 psi until it reaches the desired 20 psi and then the pressure is hold inside the actuator at this pressure. On the other hand, the deflation happens under the influence of 20 psi pressure difference which leads to a higher deflation time than inflation time.

Table 3.2.

Inflation and deflation durations of the CPIA.

Duration	Value (s)
Inflation	0.185
Deflation	0.225

From Table 3.2 it can be inferred that the inflation and deflation times fall within the swing time duration range which is 0.38s to 0.42s. Therefore, in the next chapter, mission is to design a controller to inflate and deflate the actuator at the appropriate timings to evaluate the exosuit's impact on human subjects.

Finally, to evaluate the energy consumption of the actuator, first the actuator's fully inflated volume is calculated which is found to be 283577 mm^3 . Then the energy consumption is calculated by multiplying by the operating pressure which is 20 psi. This results in 40 J approximately which is promising such that future studies can address the development of a compact and lightweight pneumatic system that enables users to wear the exosuit in home and outdoor activities.

CHAPTER 4

CONTROL AND HUMAN TESTING

4.1. Control Strategy

The controller is responsible for triggering the exosuit to deliver the required torque at the required timing. To achieve that, the control strategy illustrated in Figure 4.1 has been implemented.

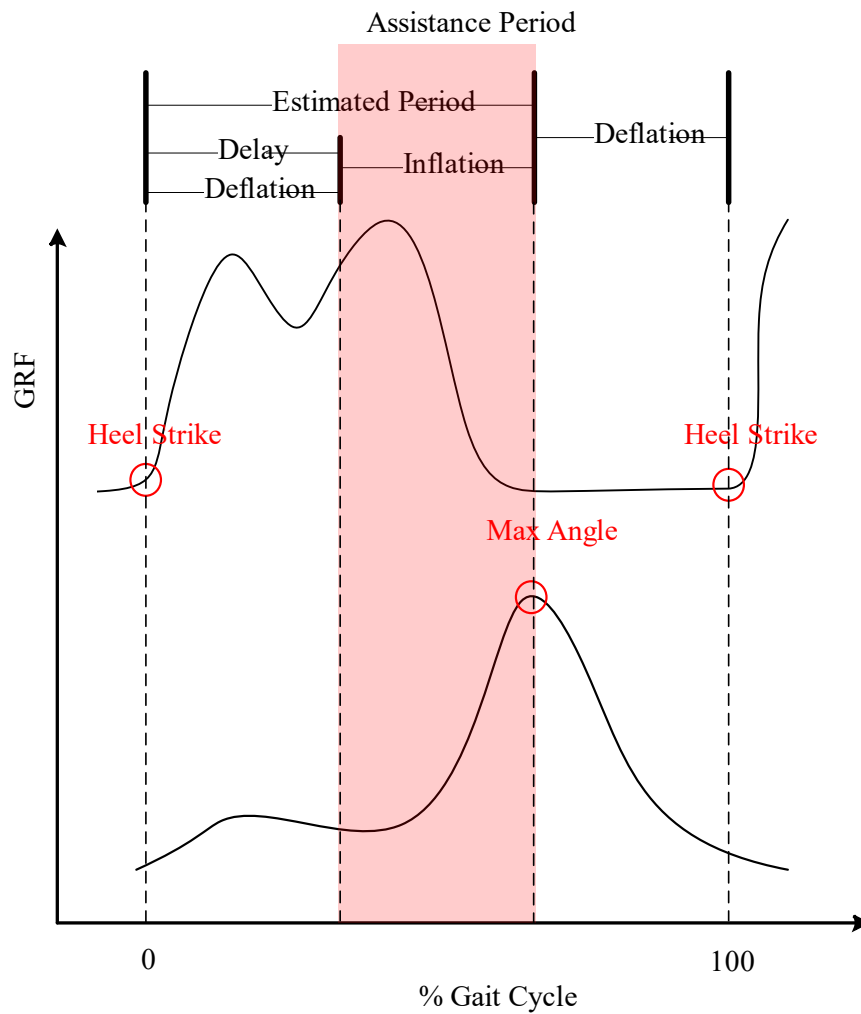


Figure 4.1. Control Strategy.

The strategy inflates the actuator after heel strike by some delay until reaches the desired pressure and holds the pressure inside the actuator until the maximum knee flexion angle and then deflates. Therefore, implementing this strategy is based on detecting the point of heel strike, the point of inflation, and the point of deflation which is the maximum knee flexion instant.

The heel strike event is detected by using a smart shoe that measures the ground reaction forces during walking. The shoe consists of 4 insole sensors distributed over the foot as described in Figure 4.2. The insole sensors are at heel, inner metatarsal, outer metatarsal, and toe. The sensors consist of coiled tubes filled with air and connected to pressure sensor to detect the pressure changes and relate to the ground reaction force. More details about the smart shoe construction and operation can be found in (Chinimilli et al., 2016). Heel strike is identified when the ground reaction force changes from 0 to greater than or equal to 10 % of the body weight.

The deflation point, maximum knee flexion, has been personalized for each subject by finding the average time from heel strike to maximum flexion of a 5-minutes baseline walking session. This has been implemented by post processing the ground reaction forces and joint angles recorded from the baseline session and averaging the estimated period duration illustrated in Figure 4.1 for all gait cycles happened during the 5-minutes walking.

Finally, detecting the inflation instant is to be determined. Ideally, the inflation instant can be evaluated by subtracting the inflation time of the actuator that has been characterized as described in Table 3.2 from the estimated period. This subtraction will result in the amount of delay required to start the inflation after heel strikes happens.

Nevertheless, that is not practically precise as there are some sources of delay in the whole system that require the inflation point to take place earlier. These source of delay result from many sources such as, the wireless communication of the smart shoes, detection of the heel strike point at 10 % of the body weight, and delays in the pneumatic circuits.

Therefore, the theoretical delay period required for inflation has been first determined for each subject by subtracting the actuator's inflation time from the estimated period, which is the duration from heel strike to maximum flexion. Then, the actual delay period has been chosen to be tuned experimentally slightly before the theoretical value to account for the delay sources in the control loop.

4.2. Hardware Setup and Components

To implement the controller, the hardware setup indicated in Figure 4.2 has been established. The control box contains the microcontroller (Raspberry Pi 3, Raspberry Pi Foundation, Cambridge, UK), electronic component like a metal-oxide-semiconductor-field-effect transistor (MOSFET), analog to digital converter, two solenoid valves (MHE3-MS1H valves, Festo, Hauppauge, NY), and a pressure sensor (ABPMANN004PGAA5, Honeywell International Inc., Morris Plains, NJ). The two solenoid valves are responsible for organizing the air flow in and out the actuator. One valve allows the flow from the air source to the actuator when it receives an on signal from the controller. The other valve is responsible for opening and closing the deflation manifold of the actuator. To accelerate the deflation of the actuator, a vacuum pump (DV-85N-250 pump, JB Industries, Aurora, IL) has been connected to the vacuum valve.

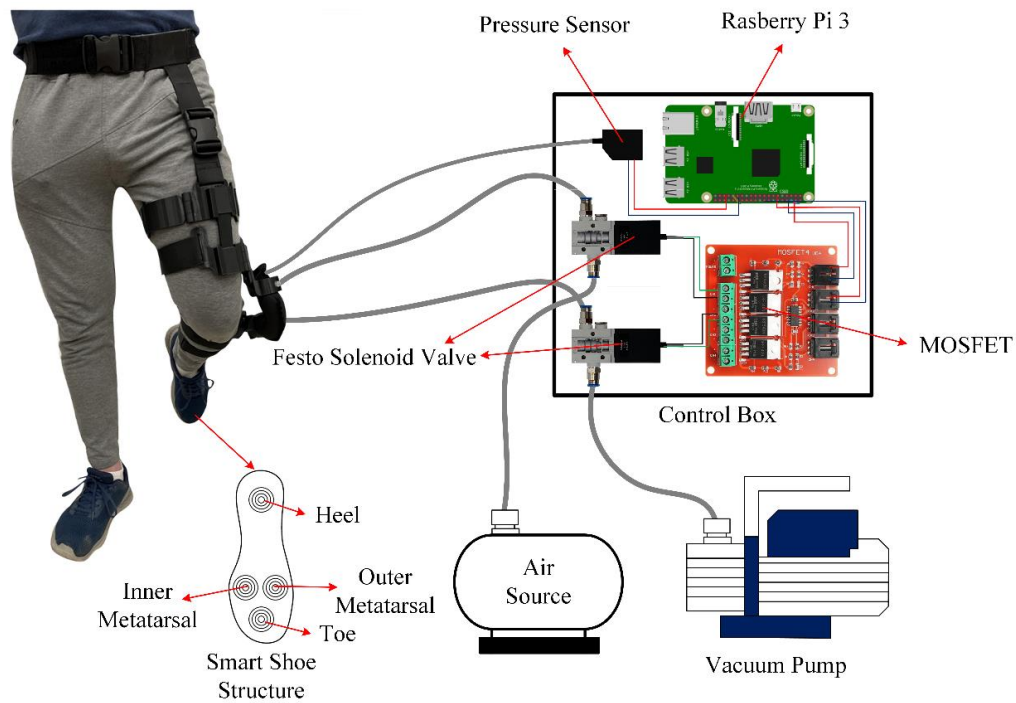


Figure 4.2. Hardware Setup and Components.

4.3. Human Testing

4.3.1. Testing Protocol

The testing protocol consists of three types of sessions namely, the baseline session, the passive session, and the active session. In the baseline session the subject walks for 5 minutes at the preferred walking speed without wearing the exosuit. During that session, the motion capture system captures the ground reaction forces and the kinematic data to calculate the estimated period to find time delay required to the controller to start the inflation cycle as discussed in section 4.2. Simultaneously, the muscle activity, electromyography (EMG), of the muscles of interest, biceps femoris, semitendinosus and vastus lateralis is recorded.

Similarly, the passive session lasts for 5 minutes of normal walking at the preferred walking speed while the subject is wearing the exosuit in the passive mode, the exosuit does not assist. The purpose of that session is to see whether the exosuit itself has effects on the muscle activity while it is on the off mode. Also, in this session, kinematic, EMG and ground reaction forces are recorded.

Finally, in the active sessions, the human subject walks for 4 sessions of 5 minutes while wearing the exosuit which actively assists the knee flexion as illustrated in Figure 4.1. The 4 sessions correspond to 4 different delay values to trigger the inflation. The delay values correspond to 35.6 %, 31.9 %, 28.1 % and 24.78 % of the gait cycle. In addition to recording kinematics, ground reaction forces and EMG data from the motion capture system, the actuator's internal pressure during the experiment has been recorded to analyze whether the control strategy achieves the required pressure and torque.

All the testing session were randomized, and they have not been performed in a certain order to counterbalance the testing conditions. After each session the subjects were asked to rest for few minutes to give time to the muscles to relax and avoid any kind of fatigue.

Before starting the sessions, the protocol has been explained to the subject and then their weights, height, leg length has been measured to set up the gait model in the motion capture system. Also, the safety precautions have been explained in detail. The subject has been asked to wear a safety harness to ensure safe walking during the experiment. After this, maximum voluntary contraction (MVC) trials have been done for EMG data

normalization. All the human experiments performed are under the institutional review boards (IRB) approval, study number: STUDY00011110.

4.3.2. Human Testing Setup

The walking experiments have been performed in the testing environment illustrated in Figure 4.3. Subjects walked on an instrumented split-belt treadmill (Bertec Inc., Columbus, OH) equipped with two force plates to measure the ground reaction forces sampled at 1000 Hz. To establish the gait model (VICON Plug-in Gait LowerBody AI), 16 reflective markers have been placed on the lower body of the subject to capture motion data at 100 Hz using the motion capture system (T40s, VICON Inc., Los Angeles, CA).

To measure the muscle's activity, EMG sensors with sampling frequency 2000 Hz (Delsys Trigno, Delsys, Natick, MA) have been placed on flexor muscles namely biceps femoris and semitendinosus as well as the vastus lateralis muscle as an extensor muscle. The EMG sensors are placed on the flexor muscles to investigate whether reduction in the activity will happen. The activity of the vastus lateralis is also recorded to see if the exosuit resists extension or not.

4.3.3. Data Processing

The ground reaction forces data is filtered using a Butterworth second order filter with a cut-off frequency 20 Hz. The EMG data is also filtered by a bandpass Butterworth 4th order filter. The data of each gait cycle (GC) is identified by detecting the heel strike points from the ground reaction forces and define the data points from heel to heel as the data of one gait cycle. To average the data of all gait cycles, a cubic spline data interpolation has been implemented on Matlab to fit the points of each gait cycle to an equal number of

data points normalized from 0 % to 100 % gait cycle. The standard deviation for the averaged data has been calculated and plotted as a shaded area around the mean curve.

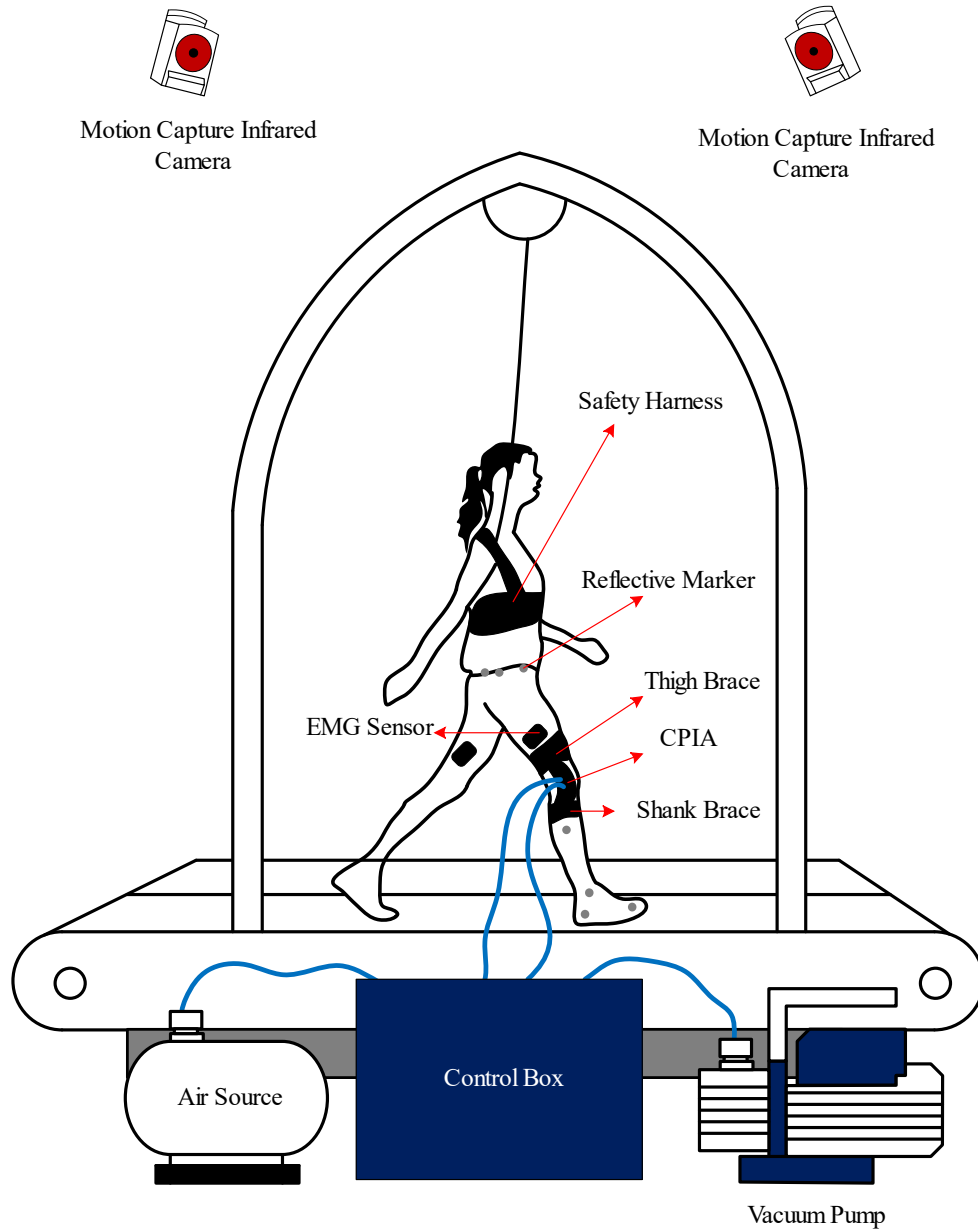


Figure 4.3. Human Testing Setup.

4.3.4. Results

The testing protocol has been performed on one human subject with information tabulated in Table 4.1. The experiment is done at 4 different delay values. The delay values are 0.4584 s, 0.4084 s, 0.3584 s and 0.3084 s. These delay values correspond to 35.6 %, 31.9 %, 28.1 % and 24.78 % of the gait cycle. The normalized EMG results with respect to the MVC of all delay trials is demonstrated in figures from Figure 4.4 to Figure 4.15.

Table 4.1.

Information of the Human Subject.

Characteristic	Value
Weight	75 Kg
Height	170 cm
Age	28 Years
Preferred Walking Speed	0.7 m/s

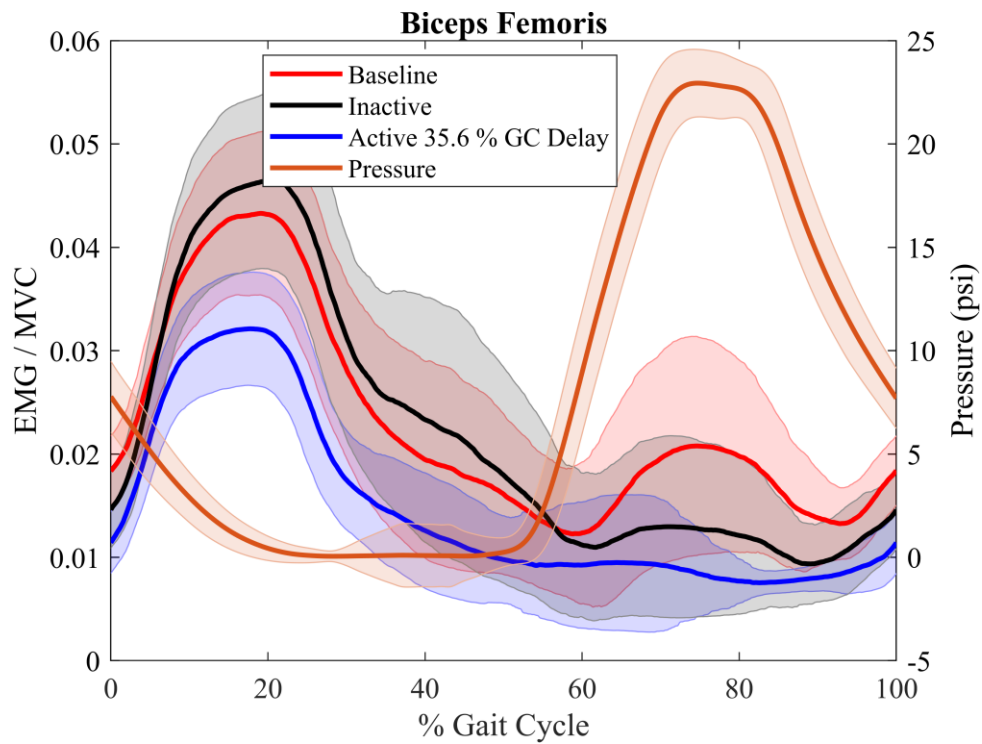


Figure 4.4. EMG of Biceps Femoris vs Actuator's Pressure at 35.6 % GC Delay.

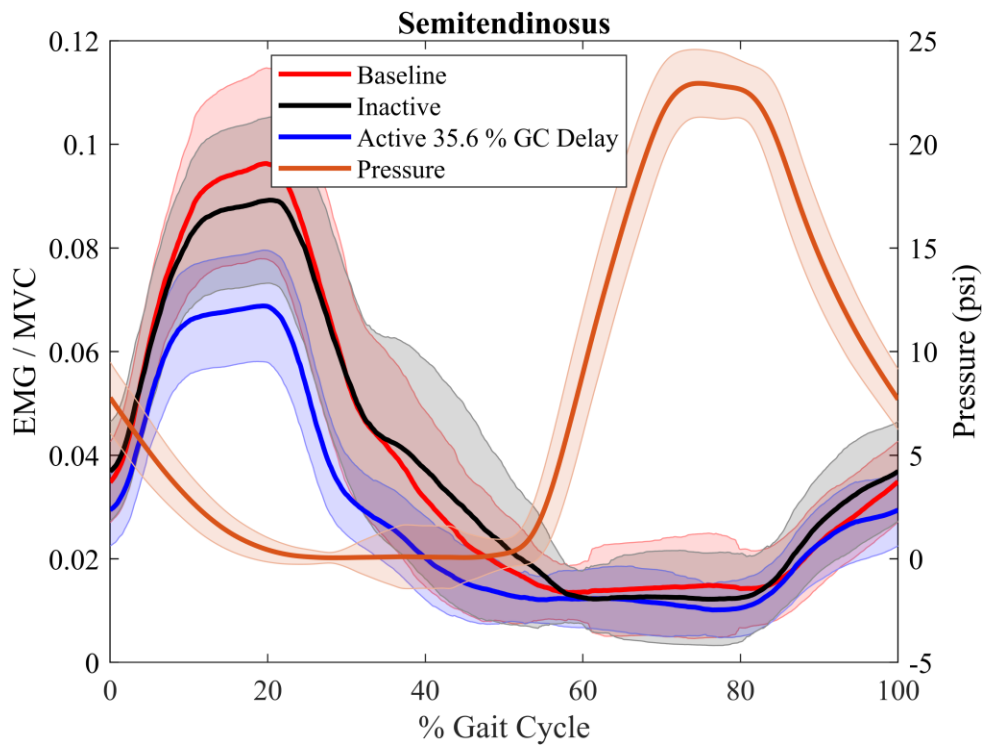


Figure 4.5. EMG of Semitendinosus Vs Actuator's Pressure at 35.6 % GC Delay.

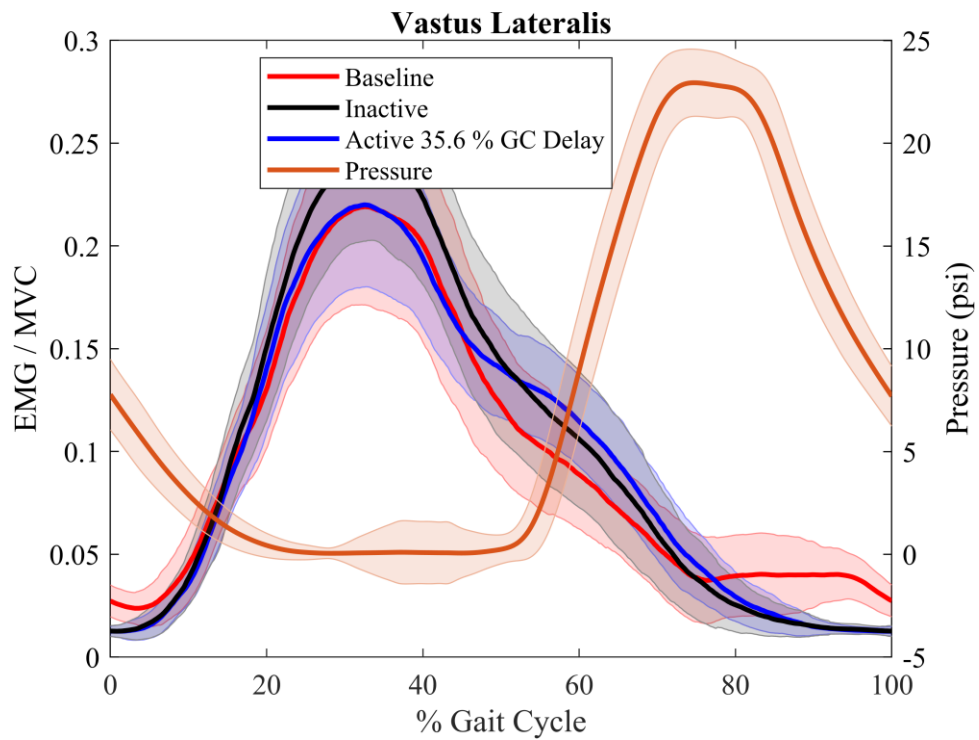


Figure 4.6. EMG of Vastus Lateralis Vs Actuator's Pressure at 35.6 % GC Delay.

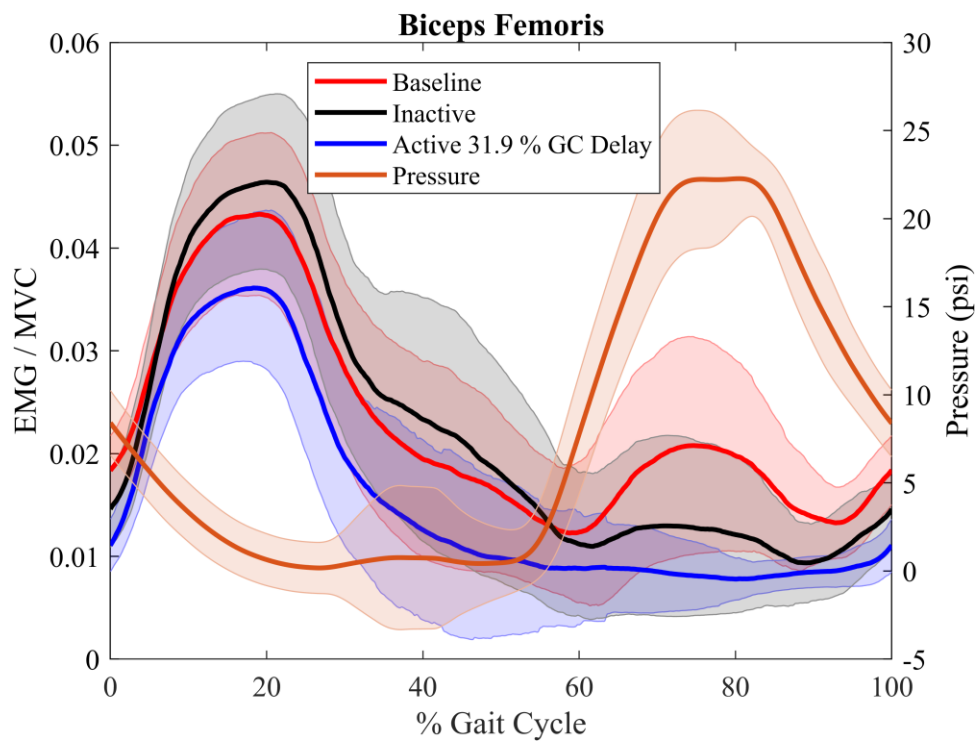


Figure 4.7. EMG of Biceps Femoris Vs Actuator's Pressure at 31.9 % GC Delay.

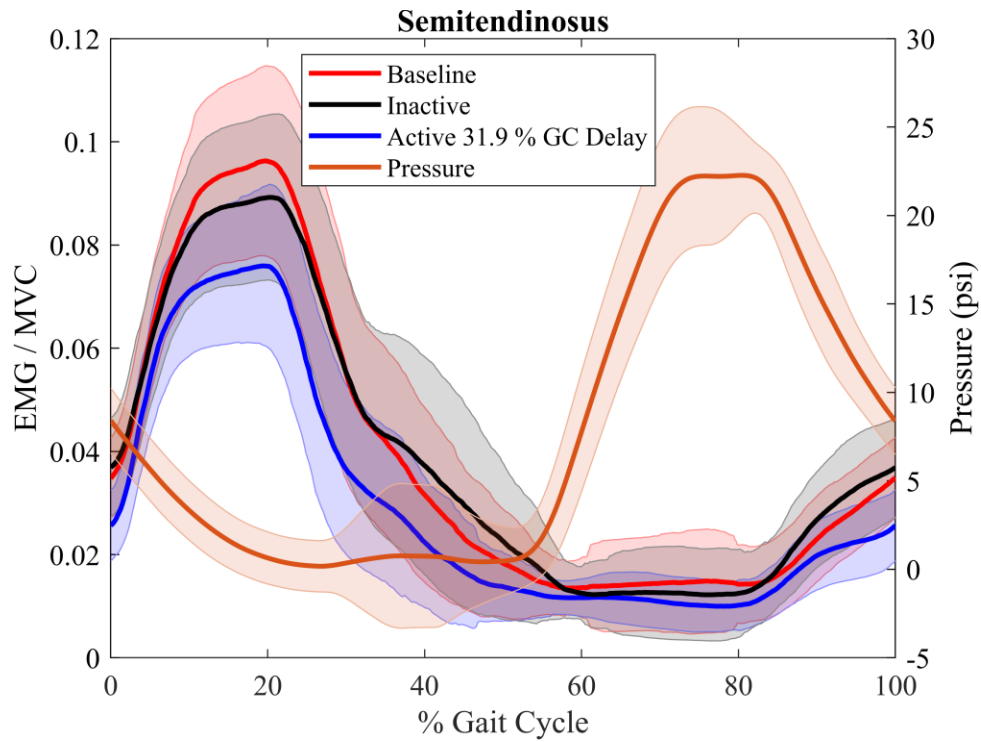


Figure 4.8. EMG of Semitendinosus Vs Actuator's Pressure at 31.9 % GC Delay.

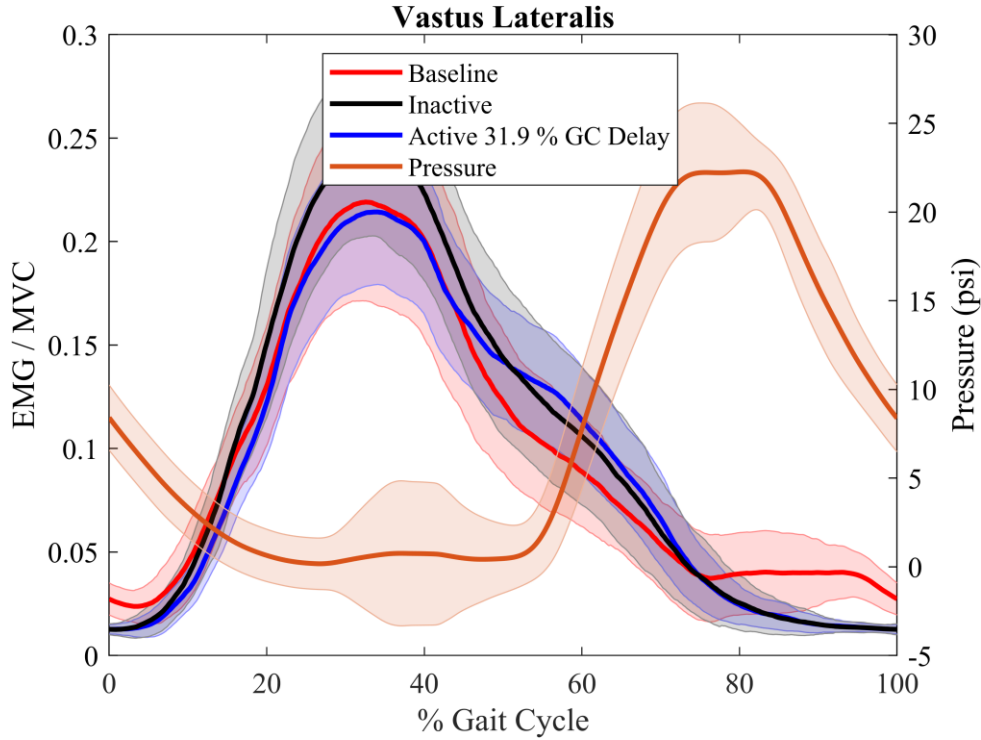


Figure 4.9. EMG of Vastus Lateralis Vs Actuators Pressure at 31.9 % GC Delay.

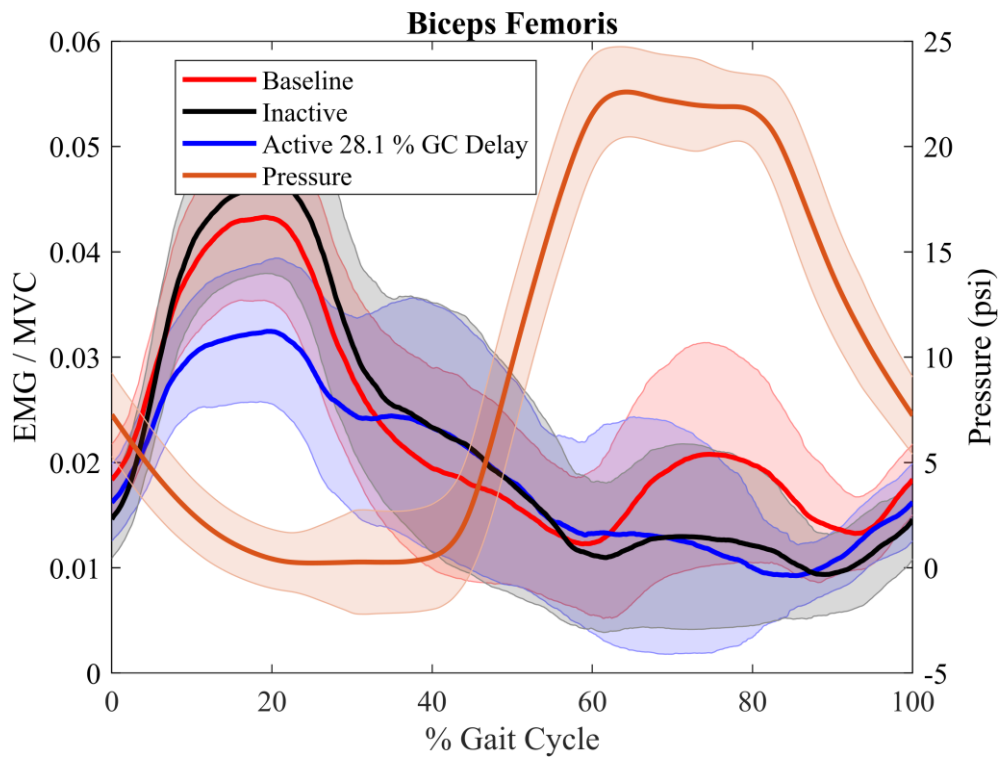


Figure 4.10. EMG of Biceps Femoris Vs Actuator's Pressure at 28.1 % GC Delay.

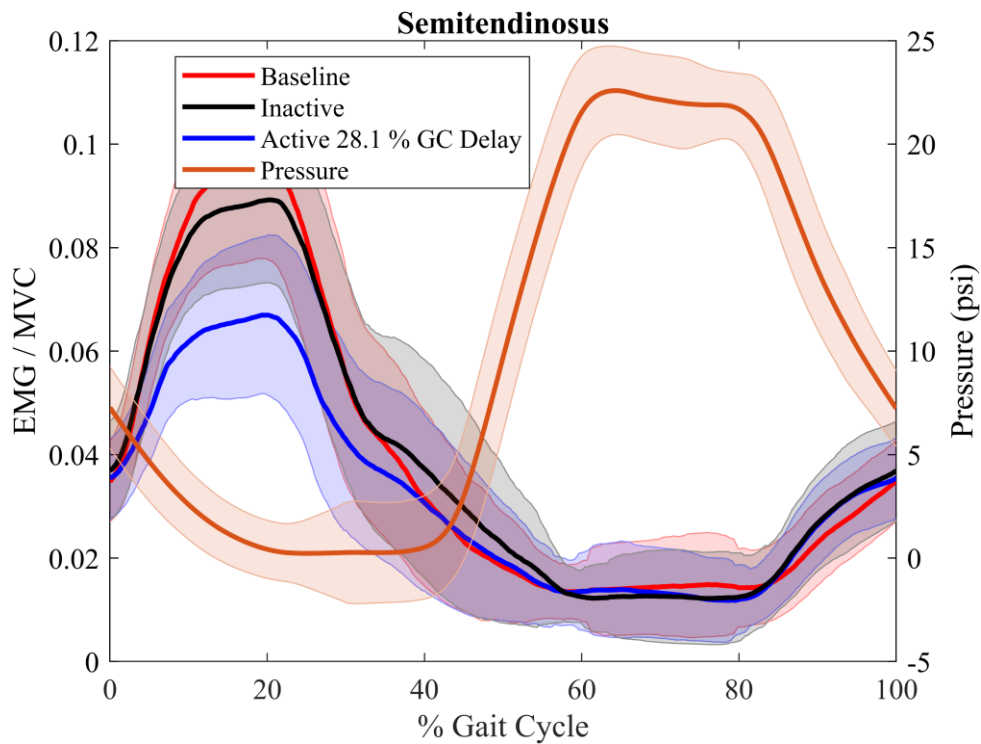


Figure 4.11. EMG of Semitendinosus Vs Actuator's Pressure at 28.1 % GC Delay.

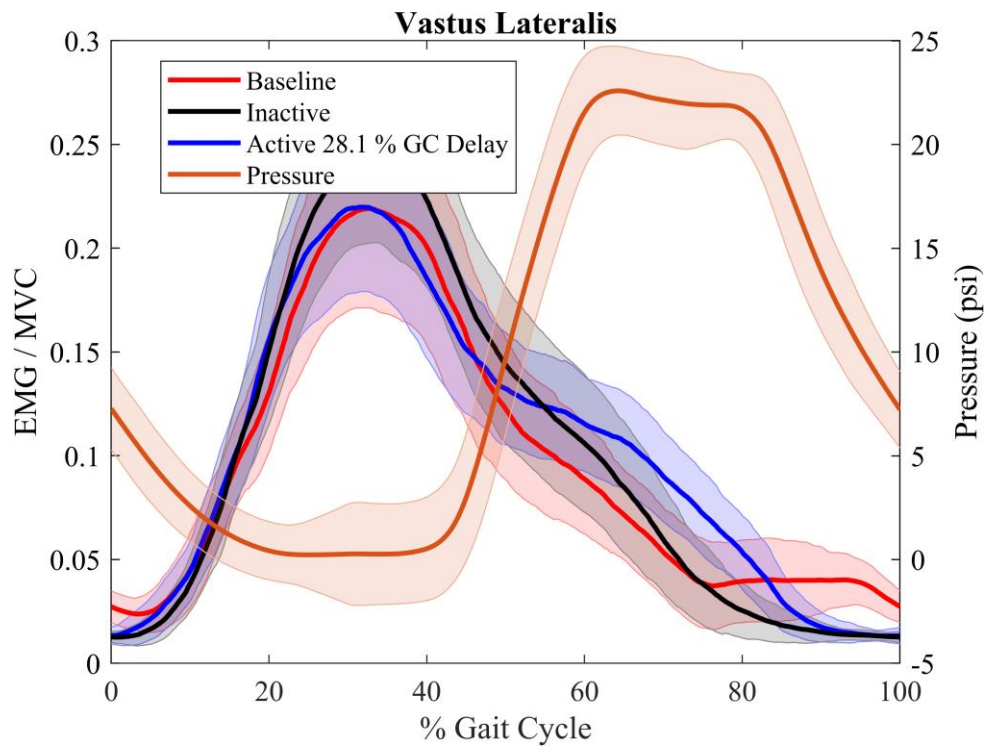


Figure 4.12. EMG of Vastus Lateralis Vs Actuator's Pressure at 28.1 % GC Delay.

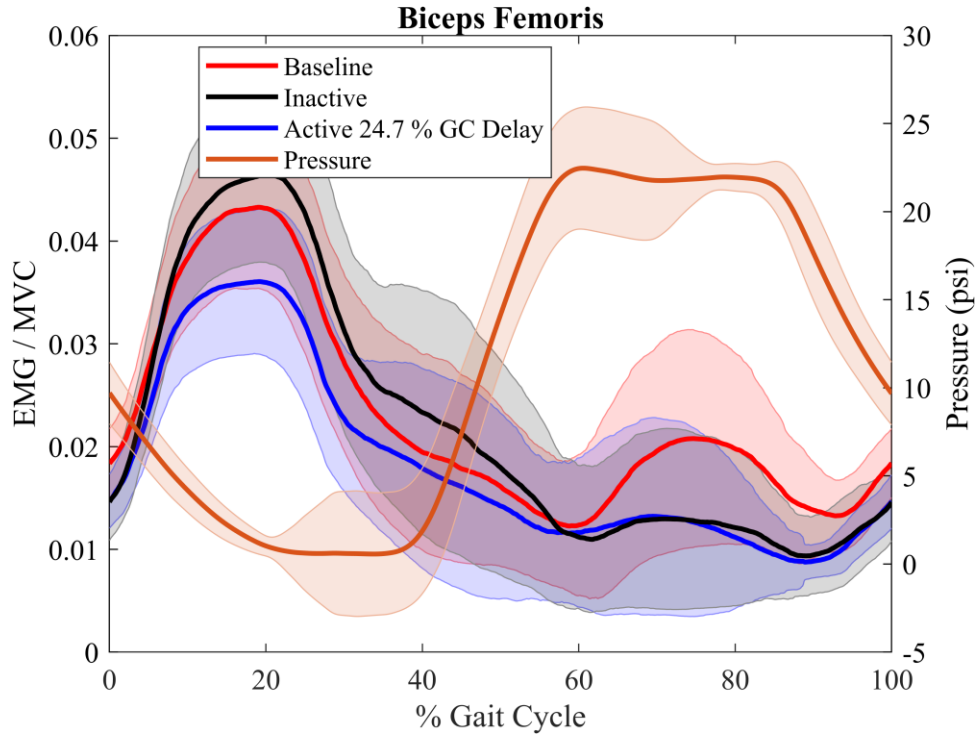


Figure 4.13. EMG of Biceps Femoris Vs Actuator's Pressure at 24.78 % GC Delay.

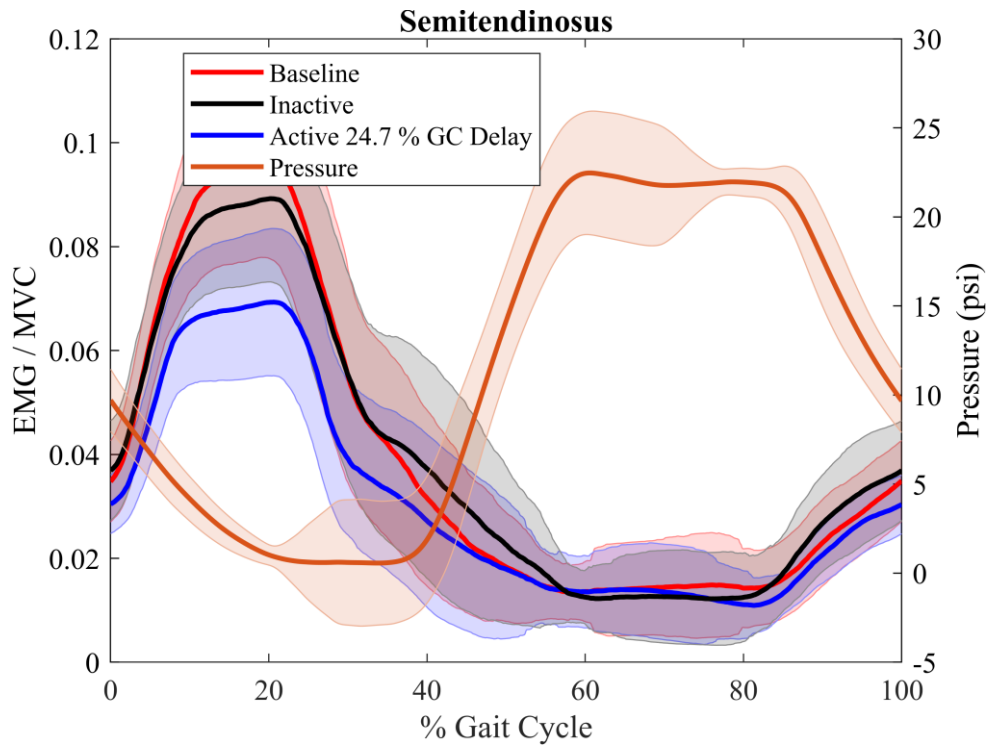


Figure 4.14. EMG of Semitendinosus Vs Actuator's Pressure at 24.78 % GC Delay.

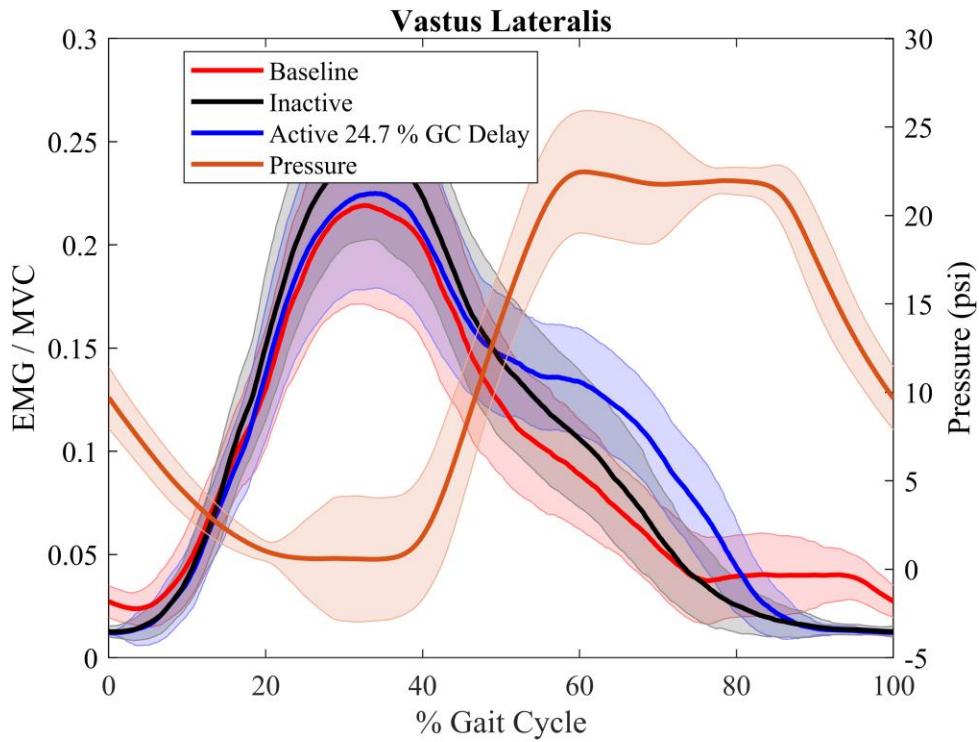


Figure 4.15. EMG of Vastus Lateralis Vs Actuator's Pressure at 24.78 % GC Delay.

4.3.5. Results Discussion

The results of the active sessions at all delays have been compared to the baseline and inactive results to investigate the effect of the exosuit on the muscles' activity. To investigate whether the exosuit is transparent to the human body, the inactive EMG results have been compared to the baseline data and the percentage change for the 3 muscles is summarized in Figure 4.16.

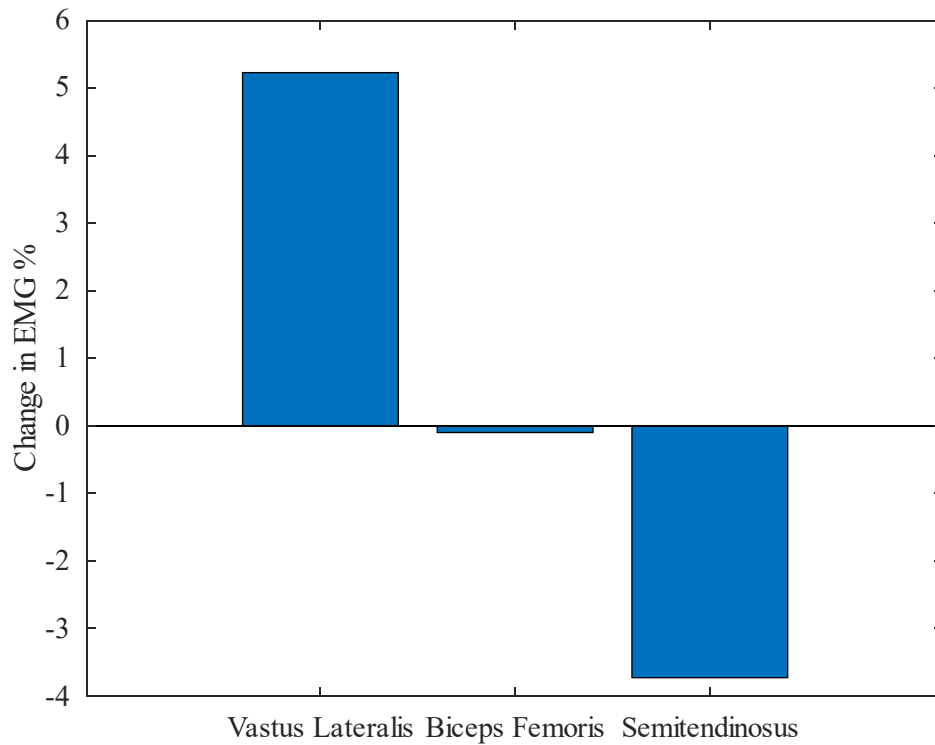


Figure 4.16. EMG Percentage Change of the Inactive Trial Compared to the Baseline.

The Inactive trial showed an average reduction of 3.73 % in the EMG of the biceps femoris and a slight average reduction of 0.1 % in the EMG of the semitendinosus while the vastus lateralis experienced a 5.23 % average increase in the EMG. However, the reduction in EMG activity of the biceps femoris and semitendinosus is relatively small in

the inactive case compared to the baseline experiment, it is unlikely expected that the exosuit reduces the EMG activity. In addition to that, the vastus lateralis experienced a significant increase in the EMG activity compared to the maximum increase experienced during the active trials which is 8.92 % when the inflation timing was set to be at 24.78 % GC. This indicates that the increase in the EMG activity mostly happens because of the interface between the human and the exosuit. This may have resulted because of the Velcro straps that are wrapped around the thigh to fix the thigh brace. Pressing on the muscles may have caused the muscle to exert more efforts at some instants and less at others which led eventually to have some reduction and increase in the muscles investigated. In the future, more investigations should be done to identify the sources of such changes that do not make the exosuit fully transparent to the body.

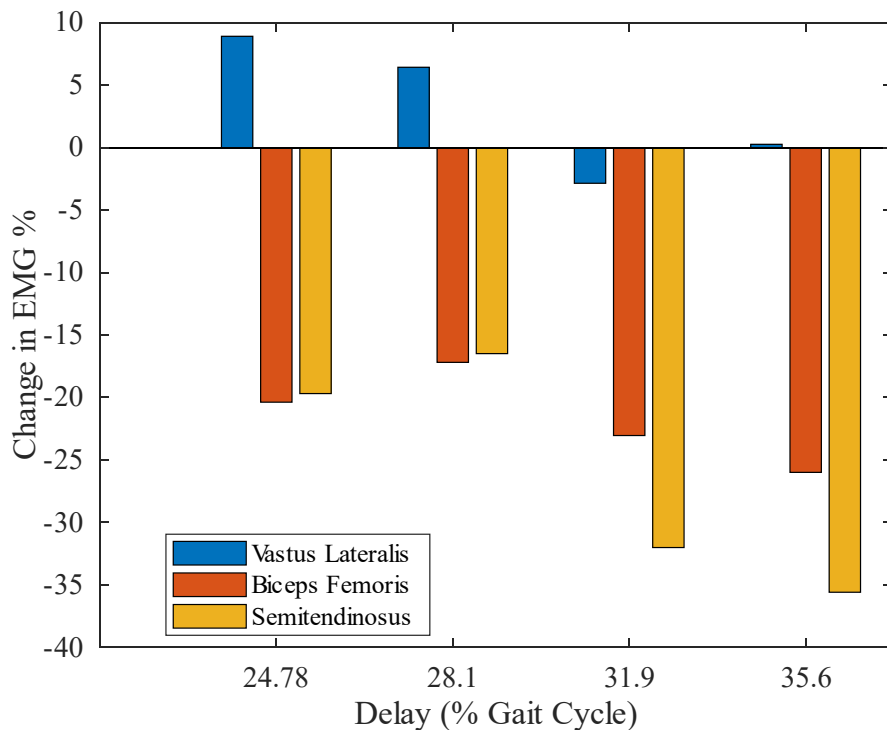


Figure 4.17. EMG Percent Change of the Active Trial Compared to the Baseline.

As illustrated in Figure 4.17, compared to the baseline experiment, EMG reduction happened in the biceps femoris and semitendinosus such that it showed the maximum at 35.6 % GC inflation timing and it increased as the delay decreased until the lowest reduction noticed at 28.1 % to increase again at 24.78 %. The active trial performed at 35.6 % GC inflation timing showed an average EMG reduction of -26 % and -35.6 % for the semitendinosus and biceps femoris respectively while the vastus lateralis exhibited a slight increase of 0.27 % in the average EMG activity. For the active session at 31.9 % GC inflation timing, the biceps femoris, the semitendinosus and the vastus lateralis all showed average EMG reduction of -32.02 %, -23.05 % and -2.85 % respectively. In the session performed at 28.1 % GC inflation timing, the biceps femoris and the semitendinosus showed -16.49 % and -17.19 % average EMG reduction respectively whereas the vastus lateralis showed more average increase in the EMG of 6.44 %. Finally, in the active session 24.7 % GC inflation timing, the biceps femoris and the semitendinosus experienced an average EMG reduction of -16.69 % and -20.38 % respectively while the vastus lateralis showed the largest average EMG increase of 8.92 %.

Compared to the inactive experiment, as demonstrated in Figure 4.18, the active session at 35.6 % GC inflation timing showed EMG reduction in all the three muscles recorded such that the biceps femoris, semitendinosus and vastus lateralis had -33.11 %, -25.93 % and -4.72 % average EMG reduction, respectively. Similarly, the active session when the delay was at 31.9 % GC inflation timing also showed reduction for all muscles of -29.38 %, -22.98 % and -7.68 % for biceps femoris, semitendinosus and vastus lateralis, respectively. On the other hand, in the active session done at 28.1 % GC inflation timing,

only biceps femoris and semitendinosus experienced EMG reduction of -13.26 % and -17.11 % respectively while the EMG of the vastus lateralis increased slightly by 1.15 %. Finally, at 24.7 % GC inflation timing, the EMG of the biceps femoris and the semitendinosus reduced by -16.58 % and -20.3 % respectively while the EMG of the vastus lateralis increased by 3.5 %.

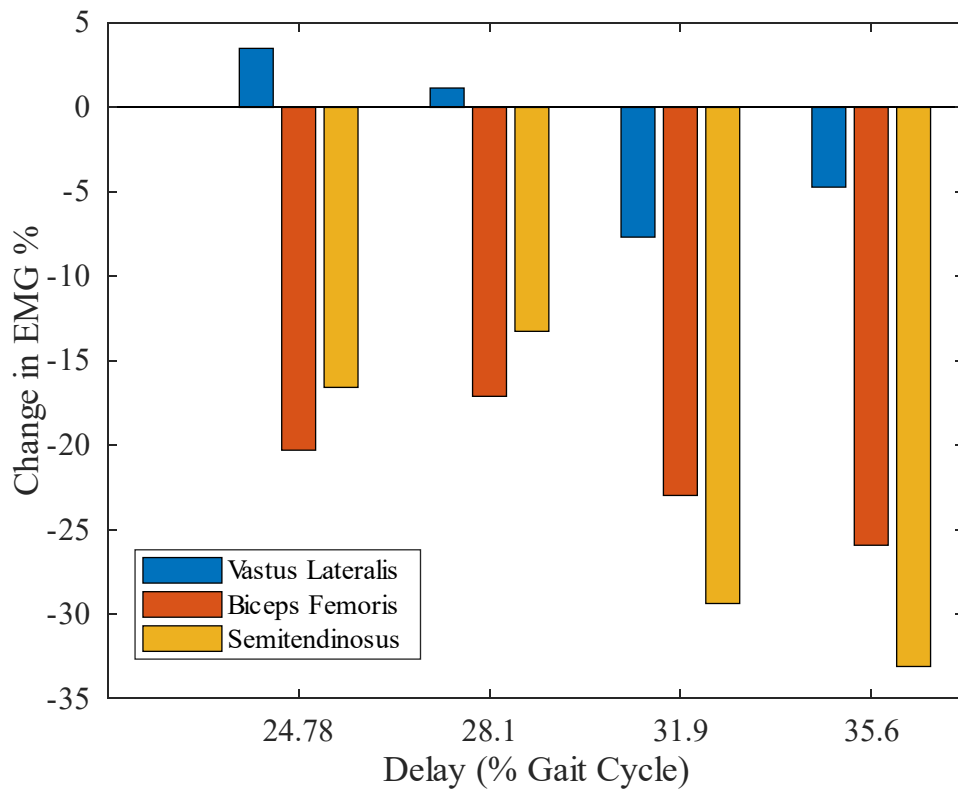


Figure 4.18. EMG Percent Change Compared of the Active Trial to the Inactive.

The increase in the EMG activity of the vastus lateralis muscle happens because the actuator is either inflated earlier before the extensor muscles deactivate and the flexor muscles. This imprecise timing in inflating makes the actuator resistant to the extension motion which increases the EMG activity as indicated in Figure 4.12 and Figure 4.15 at 28.1 % and 24.74 % GC delay consequently. Nevertheless, when the actuator inflation and

deflation cycle has been synchronized with the activation and deactivation cycle of the flexor and extensor muscles of the knee, the increase in the EMG of the vastus lateralis either vanished or had a small value as illustrated Figure 4.6 and Figure 4.9 at 35.6 % and 31.9 % GC delay consequently.

Overall, it can be concluded that compared to the baseline experiment, operating the controller at delay 0.4084 s which corresponds to 31.9 % GC gives the best performance as all flexor and extensor muscles experienced reduction in the EMG activity. On the other hand, however flexor muscles showed EMG reduction at all delay values tested, increasing the delay above or decreasing it below 31.9 % GC inflation timing leads to an increase in the EMG activity of the vastus lateralis muscle. Nevertheless, the best performance compared to the inactive trial has been obtained at 35.6 % and 31.9 % GC inflation timings such that all the muscles experienced EMG reduction. The maximum EMG reduction in the biceps femoris and the semitendinosus happened to be at 35.6 % GC inflation timing while the maximum reduction in vastus lateralis happened at 31.9 % GC inflation timing.

CHAPTER 5

CONCLUSIONS

In this research, a novel soft knee flexion exosuit has been developed. To our knowledge, the exosuit is the first soft exosuit for knee flexion assistance developed so far. A novel curved pneumatic interference actuator has been developed to generate the flexion motion required for the knee. In addition to that, two 3D printed adjustable braces have been designed and fabricated to anchor the actuator to the thigh and shank to be aligned with the knee joint. The braces showed the ability to clamp the actuator to the anchoring points efficiently such that losses in force transmission that exists in similar soft fabric braces have been eliminated.

To characterize the torque output of the actuator, an analytical model has been derived and validated experimentally. The experimental results showed that analytical model succeeded to predict the torque-pressure and torque-angle relationships at flexion angles from 0° to 60° . Above 60° , the experimental values diverged from the analytical model. This divergence happened because the actuator physically bends rather than buckles whereas the analytical model is based on modeling the torque as a function of the buckled volume. In addition to that, the analytical model showed a torque-angle trend which is like the experimental trend at all pressure values tested. Overall, analytical model derived showed the ability to predict the torque of the pneumatic interference actuator more precisely than the analytical models developed in the literature.

Furthermore, a controller has been implemented to trigger the inflate and deflate exosuit at the specific timing during the normal walking. The controller is based on

detecting the instant at which the knee starts to flex to inflate the exosuit and the instant at which maximum flexion is reached to deflate the exosuit. Those point have been detected by relating the maximum knee flexion point instant to the moment when heel strikes. Then by characterizing the inflation deflation duration of the actuator, a feedforward delay has been fed to the controller to inflate and deflate the actuator at the specified instants. As there are sources of delays in the system like the wireless communication from the smart shoe that measures the ground reaction forces, the feedforward delay has been experimentally tuned to investigate the most precise value.

After implementing the controller, the exosuit has been then tested on human subjects to evaluate its performance at the different feedforward delay values. The human experiments showed that the exosuit can assist the knee flexion such that EMG data recorded from flexor muscles namely biceps femoris and semitendinosus showed average reduction in the EMG activity in the active trials compared to the baseline and inactive trials. The results also showed that the best performance of the exosuit has been obtained by operating the controller at feedforward delay of 0.4084 s which corresponds to 31.9 % of the gait cycle. At this delay value, the flexor muscles as well as the extensor muscle investigated showed reduction in the EMG activity such that the biceps femoris and semitendinosus showed average EMG reduction of - 32.02 %, - 23.05 % and the vastus lateralis showed an average reduction of - 2.85 % respectively.

In addition to that, it is also concluded that operating the controller at imprecise feedforward delay reduces the amount of EMG reduction happens in the biceps femoris and the semitendinosus as well as increases the EMG activity of the vastus lateralis muscle.

Nevertheless, it has been noticed that the exosuit is not fully transparent to the body such that the recorded EMG data from the inactive session showed average reduction in the activity of the biceps femoris and the semitendinosus in addition to average increase in the activity of the vastus lateralis. Moreover, the vastus lateralis muscles showed an average increase in the EMG activity that is relatively near to the increase values noticed in the active cases. This concludes that the source of EMG increase of the vastus lateralis muscle happens mainly because of the exosuit interface with the human body and minorly because of the exosuit imprecise inflation and deflation timing. This behavior may have resulted from the tightening the Velcro and fabric straps used to lock the thigh brace which press on the muscle to clamp the brace with the thigh. Nevertheless, this needs to be investigated in future studies.

CHAPTER 6

FUTURE WORK

There are some challenges to be addressed in future studies to improve the analytical model. One challenge is modeling the actuator's behavior where the analytical model diverged from the experimental values. For example, modeling the output torque that has been generated from bending rather than buckling. Also, quantifying the extensibility of the fabric material and the sewing threads is another factor that needs to be considered in the analytical model. Furthermore, modifying the assumption that the actuator buckles with a circular constant-radius curved profile is expected to add significant improvements to the analytical model. In addition, designing an experimental test rig that is kinematically similar to the actuator's kinematics, in terms of having identical centers of rotation, to avoid misalignment issues during the experiments. Moreover, another development is to kinematically and mechanically program the actuator to have instantaneous centers of rotations that are identical to the instantaneous of rotations of the knee joint to ensure more anthropomorphic interaction between the exosuit and the knee joint.

Another aspect of future improvement is to develop an analytical formula that quantifies the stiffness of the actuator based on the analytical torque model derived and validate it experimentally. Having this stiffness model would allow to implement impedance controller that controls the actuator's stiffness. This impedance controller is going to be beneficial specifically for the knee joint which acts as a spring for most of the gait cycle. Also, efforts should be focused on automating the controller such that it can

robustly detect the moments when to inflated and deflate the actuator. Possible ideas for this can be integrating IMU sensors to have information about the joint angles in addition to the ground reaction forces which will enable the high-level controller to identify the events of interest more robustly. Furthermore, a biomechanical study should be designed along with clinicians to test the exosuit on a population of human subjects to have more extensive performance evaluation and to identify the areas of possible improvements. Finally, future developments should investigate the feasibility of designing a compact and lightweight pneumatic system such that a full wearable version of the exosuit can be tested on healthy and unhealthy subjects.

REFERENCES

- Armour, B. S., Courtney-Long, E. A., Fox, M. H., Fredine, H., & Cahill, A. (2016). Prevalence and causes of paralysis - United States, 2013. *American Journal of Public Health, 106*(10), 1855–1857. <https://doi.org/10.2105/AJPH.2016.303270>
- Chinimilli, P. T., Wachtel, S. W., Polygerinos, P., & Zhang, W. (2016). Hysteresis compensation for ground contact force measurement with shoe-embedded air pressure sensors. *ASME 2016 Dynamic Systems and Control Conference, DSCC 2016, 1*(September 2017). <https://doi.org/10.1115/DSCC2016-9920>
- Collins, S. H., Bruce Wiggin, M., & Sawicki, G. S. (2015). Reducing the energy cost of human walking using an unpowered exoskeleton. *Nature, 522*(7555), 212–215. <https://doi.org/10.1038/nature14288>
- Ding, Y., Galiana, I., Asbeck, A. T., De Rossi, S. M. M., Bae, J., Santos, T. R. T., De Araujo, V. L., Lee, S., Holt, K. G., & Walsh, C. (2017). Biomechanical and physiological evaluation of multi-joint assistance with soft exosuits. *IEEE Transactions on Neural Systems and Rehabilitation Engineering, 25*(2), 119–130. <https://doi.org/10.1109/TNSRE.2016.2523250>
- Fang, J., Cui, Y., Wang, M., She, S., & Yuan, J. (2018). *An Inflatable and Foldable Knee Exosuit Based on Intelligent Management of Biomechanical Energy. 12*(10), 498–501.
- Fang, J., Yuan, J., Wang, M., Xiao, L., Yang, J., Lin, Z., Xu, P., & Hou, L. (2020). Novel Accordion-Inspired Foldable Pneumatic Actuators for Knee Assistive Devices. *Soft Robotics, 7*(1), 95–108. <https://doi.org/10.1089/soro.2018.0155>
- Fasoli, S. E., Ladenheim, B., Mast, J., & Krebs, H. I. (2012). New horizons for robot-assisted therapy in pediatrics. *American Journal of Physical Medicine and Rehabilitation, 91*(11 SUPPL.3), 280–289. <https://doi.org/10.1097/PHM.0b013e31826bcff4>
- Huang, G., Ma, L., Zhu, H., Qian, Y., Leng, Y., & Fu, C. (2020). A Biologically-inspired Soft Exosuit for Knee Extension Assistance during Stair Ascent. *ICARM 2020 - 2020 5th IEEE International Conference on Advanced Robotics and Mechatronics, 570–575*. <https://doi.org/10.1109/ICARM49381.2020.9195271>
- Lee, H. D., Park, H., Seongho, B., & Kang, T. H. (2020). Development of a Soft Exosuit System for Walking Assistance During Stair Ascent and Descent. *International Journal of Control, Automation and Systems, 18*(10), 2678–2686. <https://doi.org/10.1007/s12555-019-0584-5>

- Li, S., Vogt, D. M., Rus, D., & Wood, R. J. (2017). Fluid-driven origami-inspired artificial muscles. *Proceedings of the National Academy of Sciences of the United States of America*, *114*(50), 13132–13137. <https://doi.org/10.1073/pnas.1713450114>
- Mall, N. A., Chalmers, P. N., Moric, M., Tanaka, M. J., Cole, B. J., Bach, B. R., & Paletta, G. A. (2014). Incidence and trends of anterior cruciate ligament reconstruction in the United States. *American Journal of Sports Medicine*, *42*(10), 2363–2370. <https://doi.org/10.1177/0363546514542796>
- Mansfield, P. J., & Neumann, D. A. (2019). Structure and Function of the Knee. *Essentials of Kinesiology for the Physical Therapist Assistant*, 278–310. <https://doi.org/10.1016/b978-0-323-54498-6.00010-2>
- Mooney, L. M., & Herr, H. M. (2016). Biomechanical walking mechanisms underlying the metabolic reduction caused by an autonomous exoskeleton. *Journal of NeuroEngineering and Rehabilitation*, *13*(1), 1–12. <https://doi.org/10.1186/s12984-016-0111-3>
- Murray, M. P., Kory, R. C., Clarkson, B. H., & Sepic, S. B. (1966). Comparison of Free and Fast Speed Walking Patterns of Normal Men. *American Journal of Physical Medicine*, *45*(1), 8–24.
- Nesler, C. R., Swift, T. A., & Rouse, E. J. (2018). Initial Design and Experimental Evaluation of a Pneumatic Interference Actuator. *Soft Robotics*, *5*(2), 138–148. <https://doi.org/10.1089/soro.2017.0004>
- O'Neill, C. T., McCann, C. M., Hohimer, C. J., Bertoldi, K., & Walsh, C. J. (2021). Unfolding Textile-Based Pneumatic Actuators for Wearable Applications. *Soft Robotics*, *00*(00), 1–10. <https://doi.org/10.1089/soro.2020.0064>
- Park, E. J., Akbas, T., Eckert-Erdheim, A., Sloot, L. H., Nuckols, R. W., Orzel, D., Schumm, L., Ellis, T. D., Awad, L. N., & Walsh, C. J. (2020). A Hinge-Free, Non-Restrictive, Lightweight Tethered Exosuit for Knee Extension Assistance During Walking. *IEEE Transactions on Medical Robotics and Bionics*, *2*(2), 165–175. <https://doi.org/10.1109/tmrb.2020.2989321>
- Sanchez, V., Walsh, C. J., & Wood, R. J. (2020). Textile Technology for Soft Robotic and Autonomous Garments. *Advanced Functional Materials*, *2008278*, 1–55. <https://doi.org/10.1002/adfm.202008278>
- Shamaei, K., Cenciarini, M., Adams, A. A., Gregorczyk, K. N., Schiffman, J. M., & Dollar, A. M. (2014). Design and evaluation of a quasi-passive knee exoskeleton for investigation of motor adaptation in lower extremity joints. *IEEE Transactions on Biomedical Engineering*, *61*(6), 1809–1821.

<https://doi.org/10.1109/TBME.2014.2307698>

- Shemmell, J., Johansson, J., Portra, V., Gottlieb, G. L., Thomas, J. S., & Corcos, D. M. (2007). Control of interjoint coordination during the swing phase of normal gait at different speeds. *Journal of NeuroEngineering and Rehabilitation*, 4(1), 1–14. <https://doi.org/10.1186/1743-0003-4-10>
- Sridar, S., Nguyen, P. H., Zhu, M., Lam, Q. P., & Polygerinos, P. (2017). Development of a soft-inflatable exosuit for knee rehabilitation. *IEEE International Conference on Intelligent Robots and Systems, 2017-Sept*(September), 3722–3727. <https://doi.org/10.1109/IROS.2017.8206220>
- Sridar, S., Qiao, Z., Rascon, A., Biemond, A., Beltran, A., Maruyama, T., Kwasnica, C., Polygerinos, P., & Zhang, W. (2020). Evaluating Immediate Benefits of Assisting Knee Extension With a Soft Inflatable Exosuit. *IEEE Transactions on Medical Robotics and Bionics*, 2(2), 216–225. <https://doi.org/10.1109/tmrb.2020.2988305>
- Thalman, C. M., Lam, Q. P., Nguyen, P. H., Sridar, S., & Polygerinos, P. (2018). A Novel Soft Elbow Exosuit to Supplement Bicep Lifting Capacity. *IEEE International Conference on Intelligent Robots and Systems, October*, 6965–6971. <https://doi.org/10.1109/IROS.2018.8594403>
- Van Dijk, W., & Van Der Kooij, H. (2014). XPED2: A passive exoskeleton with artificial tendons. *IEEE Robotics and Automation Magazine*, 21(4), 56–61. <https://doi.org/10.1109/MRA.2014.2360309>
- Veale, A. J., Staman, K., & van der Kooij, H. (2020). Soft, Wearable, and Pleated Pneumatic Interference Actuator Provides Knee Extension Torque for Sit-to-Stand. *Soft Robotics*, 00(00), 1–16. <https://doi.org/10.1089/soro.2019.0076>
- Yoder, P. R., Stubbs, D. M., Sawyer, K. A., & Aikens, D. (2017). Opto-mechanical design process. In *Fourth Edition: Opto-Mechanical Systems Design: Design and Analysis of Opto-Mechanical Assemblies* (Vol. 1). <https://doi.org/10.1201/b18147>
- Zhang, L., Liu, G., Han, B., Wang, Z., Yan, Y., Ma, J., & Wei, P. (2020). Knee Joint Biomechanics in Physiological Conditions and How Pathologies Can Affect It: A Systematic Review. *Applied Bionics and Biomechanics*, 2020. <https://doi.org/10.1155/2020/7451683>
- Zoss, A. B., Kazerooni, H., & Chu, A. (2006). Biomechanical design of the Berkeley Lower Extremity Exoskeleton (BLEEX). *IEEE/ASME Transactions on Mechatronics*, 11(2), 128–138. <https://doi.org/10.1109/TMECH.2006.871087>

APPENDIX A
DESCISION MATRICES

I. MATRIX DESCRIPTION

Criteria

The decision matrix evaluates the 3 concepts based on the following criteria,

- Inflation/ Deflation duration. By roughly evaluating the 3 concepts, which one is going to be the fastest to inflated and deflate.
- Anthropomorphic. Which actuator matches well with the geometry of the knee joint and is going to be comfortably integrated on mounted on it.
- Manufacturability. Which one is going to be the easiest to manufacture?

Weights

Inf/Def Duration = 50,

Anthropomorphism= 30,

Maufacurability= 20.

II. EVALUATOR I

Issue:		PAM	Accordion- Inspired	CPIA
Choosing a Knee Flexion Actuator				
Inf/Def Duration	50	1	-1	1
Anthropomorphism	30	-1	0	0
Manufacurability	20	-1	-1	1
Total		-1	-2	2
Weighted Total		0	-70	70

III. EVALUATOR II

Issue:		PAM	Accordion- Inspired	CPIA
Choosing a Knee Flexion Actuator				
Inf/Def Duration	50	0	-1	0
Anthropomorphism	30	1	1	1
Manufacturability	20	0	-1	1
Total		1	-1	2
Weighted Total		30	-40	50

IV. EVALUATOR III

Issue: Choosing a Knee Flexion Actuator		PAM	Accordion- Inspired	CPIA
Inf/Def Duration	50	1	-1	1
Anthropomorphism	30	0	1	1
Manufacurability	20	1	-1	1
Total		2	-1	3
Weighted Total		70	-40	100

V. EVALUATOR IV

Issue:		PAM	Accordion - Inspired	CPIA
Choosing a Knee Flexion Actuator				
Inf/Def Duration	50	0	-1	0
Anthropomorphism	30	-1	0	1
Manufacurability	20	1	0	1
Total		0	-1	2
Weighted Total		-10	-50	50

VI. EVALUATOR V

Issue: Choosing a Knee Flexion Actuator		PAM	Accordion - Inspired	CPIA
Inf/Def Duration	50	1	0	1
Anthropomorphic	30	0	0	0
Manufacturability	20	0	-1	0
Total		1	-1	1
Weighted Total		50	-20	50